ASTROBIOLOGY
Volume 11, Number 5, 2011

DOI: 10.1089/ast.2010.0509

Using Biogenic Sulfur Gases as Remotely Detectable Biosignatures on Anoxic Planets

Shawn D. Domagal-Goldman,[1] Victoria S. Meadows,[2,3] Mark W. Claire,[2,3] and James F. Kasting[3,4]

Abstract

We used one-dimensional photochemical and radiative transfer models to study the potential of organic sulfur compounds (CS_2, OCS, CH_3SH, CH_3SCH_3, and $CH_3S_2CH_3$) to act as remotely detectable biosignatures in anoxic exoplanetary atmospheres. Concentrations of organic sulfur gases were predicted for various biogenic sulfur fluxes into anoxic atmospheres and were found to increase with decreasing UV fluxes. Dimethyl sulfide (CH_3SCH_3, or DMS) and dimethyl disulfide ($CH_3S_2CH_3$, or DMDS) concentrations could increase to remotely detectable levels, but only in cases of extremely low UV fluxes, which may occur in the habitable zone of an inactive M dwarf. The most detectable feature of organic sulfur gases is an indirect one that results from an increase in ethane (C_2H_6) over that which would be predicted based on the planet's methane (CH_4) concentration. Thus, a characterization mission could detect these organic sulfur gases—and therefore the life that produces them—if it could sufficiently quantify the ethane and methane in the exoplanet's atmosphere. Key Words: Exoplanets—Biosignatures—Anoxic atmospheres—Planetary atmospheres—Remote life detection—Photochemistry. Astrobiology 11, 419–441.

1. Introduction

The search for life may soon expand beyond the boundaries of our solar system via the detection of spectral features of "biosignature" gases on extrasolar planets (European Space Agency, 2010; Jet Propulsion Laboratory, 2010; New Worlds Observer Team, 2010). For a gas to be a biosignature it must have a biological production rate that far outpaces abiotic sources and an atmospheric lifetime that allows it to build up to detectable levels. To be detectable, the biosignature gas must have spectral features that are (1) within a wavelength region that can be covered by instrumentation, (2) larger than the signal-to-noise ratio (S/N) for these instruments, and (3) distinguishable from other spectral features.

For biospheres in which primary productivity is dominated by oxygenic photosynthesis (henceforth referred to as "oxic" biospheres), a number of gases have been identified that meet these criteria: oxygen (O_2), ozone (O_3), or both in the presence of reduced species such as methane (CH_4) (Lovelock, 1965; Des Marais *et al.,* 2002); nitrous oxide (N_2O) (Sagan *et al.,* 1993); and methyl chloride (CH_3Cl) (Segura *et al.,* 2005). The latter two gases are more difficult to detect in Earth's present atmosphere than are the first two; however, they might be more visible in the atmospheres of oxic Earth-like planets orbiting M stars due to longer atmospheric lifetimes resulting from lower photolysis rates (Segura *et al.,* 2005).

Other biosignatures are needed for detection of "anoxic biospheres" that harbor life but not detectable amounts of atmospheric O_2 and O_3. Biogenic CH_4 could be abundant enough to be detectable in such an atmosphere (Kasting *et al.,* 1983, 2001; Kasting, 2005; Kharecha *et al.,* 2005; Kaltenegger *et al.,* 2007), but its interpretation would be ambiguous because abiotic processes such as serpentinization can also produce CH_4 (Berndt *et al.,* 1996; Kasting and Catling, 2003).

From the early history of life on Earth, we know that anoxic biospheres are possible. Studies of early Earth suggest that life was present well before significant O_2 accumulated in the atmosphere (Schopf, 1983; Holland, 1984; Farquhar and Wing, 2003; Westall, 2005; Farquhar *et al.,* 2007). This period had vigorous biological activity without significant O_2 buildup and may have lasted as long as 1.5 billion years, approximately one-third of Earth's history. This suggests that planets with life, but without O_2/O_3, could represent a large fraction of inhabited planets. Thus, the absence of

[1]NASA Headquarters, Washington DC.
[2]Astronomy Department, University of Washington, Seattle, Washington.
[3]NASA Astrobiology Institute.
[4]Department of Geosciences, The Pennsylvania State University, University Park, Pennsylvania.

Table 1. List of Reactions in the Photochemical Code, along with the Reaction Rate Constants Used and a Source for the Reaction Rate Constant

Rxn. #	*Reaction*	*Reaction rate constant*	*Reference*
1	$OCS + CH \rightarrow CO + HCS$	$1.99 \cdot 10^{-10} \times e^{-190/T}$	Zabarnick *et al.*, 1989
2	$OCS + H \rightarrow CO + HS$	$9.07 \cdot 10^{-12} \times e^{-1940/T}$	Lee *et al.*, 1977
3	$OCS + O \rightarrow S + CO_2$	$8.3 \cdot 10^{-11} \times e^{-5530/T}$	Singleton and Cvetanovic, 1988
4	$OCS + O \rightarrow SO + CO$	$2.1 \cdot 10^{-11} \times e^{-2200/T}$	Toon *et al.*, 1987
5	$OCS + OH \rightarrow CO_2 + HS$	$1.1 \cdot 10^{-13} \times e^{-1200/T}$	Atkinson *et al.*, 2004
6	$OCS + OH \rightarrow HS + CO_2$	$1.1 \cdot 10^{-13} \times e^{-1200/T}$	Atkinson *et al.*, 2004
7	$OCS + S \rightarrow CO + S_2$	$1.5 \cdot 10^{-10} \times e^{-1830/T}$	Schofield, 1973
8	$OCS + S + M \rightarrow OCS_2 + M$	$8.3 \cdot 10^{-33} \times den$	Basco and Pearson, 1967
9	$OCS_2 + CO \rightarrow OCS + OCS$	$3.0 \cdot 10^{-12}$	Zahnle *et al.*, 2006
10	$OCS_2 + S \rightarrow OCS + S_2$	$2.0 \cdot 10^{-11}$	Zahnle *et al.*, 2006
11	$C_2H_6S + CH_3 \rightarrow CH_4 + C_2H_4 + HS$	$6.92 \cdot 10^{-13} \times e^{-4610/T}$	Arthur and Lee, 1976
12	$C_2H_6S + H \rightarrow C_2H_5 + H_2S$	$8.49 \cdot 10^{-12} \times e^{-1200/T}$	Lam *et al.*, 1989
13	$C_2H_6S + H \rightarrow CH_3SH + CH_3$	$4.81 \cdot 10^{-12} \times e^{-1100/T} \times (T/300)^{1.7}$	Zhang *et al.*, 2005
14	$C_2H_6S + H \rightarrow H_2 + C_2H_4 + HS$	$8.34 \cdot 10^{-12} \times e^{-2212/T} \times (T/300)^{1.6}$	Zhang *et al.*, 2005
15	$C_2H_6S + OH \rightarrow H_2O + C_2H_4 + HS$	$1.13 \cdot 10^{-11} \times e^{-253/T}$	Atkinson *et al.*, 2004
16	$C_2H_6S_2 + H \rightarrow CH_3SH + CH_3S$	$9.47 \cdot 10^{-12} \times e^{-50/T}$	Ekwenchi *et al.*, 1980
17	$CH_3 + HS \rightarrow CH_3SH$	$1.66 \cdot 10^{-11}$	Shum and Benson, 1985
18	$CH_3S + CH_3S \rightarrow C_2H_6S_2$	$4.00 \cdot 10^{-11}$	Anastasi *et al.*, 1991
19	$CH_3S + CO \rightarrow CH_3 + OCS$	$2.6 \cdot 10^{-11} \times e^{-5940/T}$	Assumed same as $k(CH_3O + CO)$
20	$CH_3S + CS \rightarrow CH_3 + CS_2$	$2.6 \cdot 10^{-11} \times e^{-5940/T}$	Assumed same as $k(CH_3O + CO)$
21	$CH_3S + H_2O_2 \rightarrow CH_3SH + H_2O$	$3.01 \cdot 10^{-13}$	Turnipseed *et al.*, 1996
22	$CH_3S + HCS \rightarrow CH_3SH + CS$	$1.18 \cdot 10^{-12} \times e^{-910/T} \times (T/300)^{0.65}$	Liu *et al.*, 2006
23	$CH_3S + HS \rightarrow CH_3SH + S$	$1.66 \cdot 10^{-11}$	Assumed same as $k(CH_3 + HS)$
24	$CH_3SH + CH_3 \rightarrow CH_4 + CH_3S$	$2.99 \cdot 10^{-31}$	Kerr and Trotman-Dickenson, 1957
25	$C_2H_6S + O \rightarrow CH_3 + CH_3 + SO$	$1.30 \cdot 10^{-11} \times e^{-410/T} \times (T/298)^{1.1}$	Sander *et al.*, 2006
26	$CH_3SH + O \rightarrow CH_3 + HSO$	$1.30 \cdot 10^{-11} \times e^{-410/T} \times (T/298)^{1.1}$	Assumed same as $k(C_2H_6S + O)$
27	$C_2H_6S_2 + O \rightarrow CH_3 + CH_3S + SO$	$3.90 \cdot 10^{-11} \times e^{290/T} \times (T/298)^{1.1}$	Sander *et al.*, 2006
28	$C_2H_6S + OH \rightarrow CH_2^1 + CH_3S + H_2O$	$1.10 \cdot 10^{-11} \times e^{-240/T} \times (T/298)^{1.1}$	Sander *et al.*, 2006
29	$C_2H_6S_2 + OH \rightarrow CH_3 + CH_3SH + SO$	$6.00 \cdot 10^{-11} \times e^{400/T} \times (T/298)^{1.2}$	Sander *et al.*, 2006
30	$CH_3SH + OH \rightarrow CH_3S + H_2O$	$9.90 \cdot 10^{-12} \times e^{360/T} \times (T/298)^{1.07}$	Sander *et al.*, 2006
31	$C_2H_6S + O \rightarrow CH_3 + CH_3 + SO$	$1.30 \cdot 10^{-11} \times e^{-410/T} \times (T/298)^{1.1}$	Sander *et al.*, 2006
32	$CH_3SH + O \rightarrow CH_3 + HSO$	$1.30 \cdot 10^{-11} \times e^{-410/T} \times (T/298)^{1.1}$	Assumed same as $k(C_2H_6S + O)$
33	$CH_3SH + H \rightarrow CH_3 + H_2S$	$1.5 \cdot 10^{-11} \times e^{-840/T}$	Amano *et al.*, 1983
34	$CH_3SH + H \rightarrow H_2 + CH_3S$	$4.82 \cdot 10^{-11} \times e^{-1310/T}$	Amano *et al.*, 1983
35	$CH_3SH + OH \rightarrow H_2O + CH_3S$	$9.9 \cdot 10^{-12} \times e^{360/T}$	DeMore and Yung, 1982
36	$CH + CS_2 \rightarrow HCS + CS$	$3.49 \cdot 10^{-10} \times e^{-40/T}$	Zabarnick *et al.*, 1989
37	$CS + HS \rightarrow CS_2 + H$	$1.5 \cdot 10^{-13} \times (1 + 0.6 \times den)$	Assumed same as $k(CO + OH)$
38	$CS + O \rightarrow CO + S$	$2.7 \cdot 10^{-10} \times e^{-760/T}$	Atkinson *et al.*, 2004
39	$CS + O_2 \rightarrow CO + SO$	$5 \cdot 10^{-20}$	Wine *et al.*, 1981
40	$CS + O_2 \rightarrow OCS + O$	$4 \cdot 10^{-19}$	Wine *et al.*, 1981
41	$CS + O_3 \rightarrow CO + SO_2$	$3 \cdot 10^{-12}$	Wine *et al.*, 1981
42	$CS + O_3 \rightarrow OCS + O_2$	$3 \cdot 10^{-12}$	Wine *et al.*, 1981
43	$CS + O_3 \rightarrow SO + CO_2$	$3 \cdot 10^{-12}$	Wine *et al.*, 1981
44	$CS_2 + O \rightarrow CO + S_2$	$5.81 \cdot 10^{-14}$	Singleton and Cvetanovic, 1988
45	$CS_2 + O \rightarrow OCS + S$	$3 \cdot 10^{-12} \times e^{-650/T}$	Toon *et al.*, 1987
46	$CS_2 + O \rightarrow SO + CS$	$3.2 \cdot 10^{-11} \times e^{-650/T}$	Toon *et al.*, 1987
47	$CS_2 + OH \rightarrow OCS + HS$	$2 \cdot 10^{-15}$	Atkinson *et al.*, 2004
48	$CS_2 + S \rightarrow CS + S_2$	$1.9 \cdot 10^{-14} \times e^{-580/T} \times (T/300)^{3.97}$	Woiki and Roth, 1995
49	$CS_2 + SO \rightarrow OCS + S_2$	$2.4 \cdot 10^{-13} \times e^{-2370/T}$	Assumed same as $k(SO^* + O_2)$
50	$CS_2^* + CS_2 \rightarrow CS + CS + S_2$	$1 \cdot 10^{-12}$	Assumed same as $k(CS_2^* + CS_2$
51	$CS_2^* + M \rightarrow CS_2 + M$	$2.5 \cdot 10^{-11}$	Wine *et al.*, 1981
52	$CS_2^* + O_2 \rightarrow CS + SO_2$	$1 \cdot 10^{-12}$	Wine *et al.*, 1981
53	$C + HS \rightarrow CS + H$	$4 \cdot 10^{-11}$	Assumed same as $k(C + OH)$
54	$C + S_2 \rightarrow CS + S$	$3.3 \cdot 10^{-11}$	Assumed same as $k(C + O_2)$
55	$C_2 + S \rightarrow C + CS$	$5 \cdot 10^{-11}$	Assumed same as $k(C_2 + O)$
56	$C_2 + S_2 \rightarrow CS + CS$	$1.5 \cdot 10^{-11} \times e^{-550/T}$	Assumed same as $k(C_2 + O_2)$
57	$CH + S \rightarrow CS + H$	$9.5 \cdot 10^{-11}$	Assumed same as $k(CH + CS_2)$
58	$CH + S_2 \rightarrow CS + HS$	$5.9 \cdot 10^{-11}$	Assumed same as $k(CH + O_2)$
59	$CH_2^1 + S_2 \rightarrow HCS + HS$	$3 \cdot 10^{-11}$	Assumed same as $k(CH_2^1 + O_2)$
60	$CH_3 + HCS \rightarrow CH_4 + CS$	$8.2 \cdot 10^{-11}$	Assumed same as $k(CH_3 + HCO)$
61	$H + CS + M \rightarrow HCS + M$	$2.0 \cdot 10^{-33} \times e^{-850/T} \times den$	Assumed same as $k(H + CO)$

(*continued*)

Table 1. (Continued)

Rxn. #	*Reaction*	*Reaction rate constant*	*Reference*
62	$H + HCS \rightarrow H_2 + CS$	$1.2 \cdot 10^{-10}$	Assumed same as *k*(H + HCO)
63	$HS + CO \rightarrow OCS + H$	$4.2 \cdot 10^{-14} \times e^{-7650/T}$	Kurbanov and Mamedov, 1995
64	$HS + HCS \rightarrow H_2S + CS$	$5.0 \cdot 10^{-11}$	Assumed same as *k*(HS + HCO)
65	$OCS + CH \rightarrow CO + HCS$	$1.99 \cdot 10^{-10} \times e^{-190/T}$	Zabarnick *et al.*, 1989
66	$S + CO + M \rightarrow OCS + M$	$6.5 \cdot 10^{-33} \times e^{-2180/T} \times den$	Assumed same as *k*(CO + O)
67	$S + HCS \rightarrow H + CS_2$	$1.0 \cdot 10^{-10}$	Assumed same as *k*(O + HCO → H + CO_2)
68	$S + HCS \rightarrow HS + CS$	$5.0 \cdot 10^{-11}$	Assumed same as *k*(O + HCO → HS + CO)
69	$2CH_2^3 \rightarrow C_2H_2 + H_2$	$5.3 \cdot 10^{-11}$	Braun *et al.*, 1970
70	$C + H_2 + M \rightarrow CH_2^3 + M$	$k_0 = 8.75 \cdot 10^{-31} \times e^{524/T}$ $k_\infty = 8.3 \cdot 10^{-1}$	Zahnle, 1986
71	$C + O_2 \rightarrow CO + O$	$3.3 \cdot 10^{-11}$	Donovan and Husain, 1970
72	$C + OH \rightarrow CO + H$	$4 \cdot 10^{-11}$	Giguere and Huebner, 1978
73	$C_2 + CH_4 \rightarrow C_2H + CH_3$	$5.05 \cdot 10^{-11} \times e^{-297/T}$	Pitts *et al.*, 1982
74	$C_2 + H_2 \rightarrow C_2H + H$	$1.77 \cdot 10^{-10} \times e^{-1469/T}$	Pitts *et al.*, 1982
75	$C_2 + O \rightarrow C + CO$	$5 \cdot 10^{-11}$	Prasad and Huntress, 1980
76	$C_2 + O_2 \rightarrow CO + CO$	$1.5 \cdot 10^{-11} \times e^{-550/T}$	Baughcum and Oldenborg, 1984
77	$C_2H + C_2H_2 \rightarrow HCAER + H$	$1.5 \cdot 10^{-10}$	Stephens *et al.*, 1987
78	$C_2H + C_2H_6 \rightarrow C_2H_2 + C_2H_5$	$3.6 \cdot 10^{-11}$	Lander *et al.*, 1990
79	$C_2H + C_3H_8 \rightarrow C_2H_2 + C_3H_7$	$1.4 \cdot 10^{-11}$	Okabe, 1983
80	$C_2H + CH_2CCH_2 \rightarrow HCAER + H$	$1.5 \cdot 10^{-10}$	Pavlov *et al.*, 2001
81	$C_2H + CH_4 \rightarrow C_2H_2 + CH_3$	$6.94 \cdot 10^{-12} \times e^{-250/T}$	Allen *et al.*, 1992; Lander *et al.*, 1990
82	$C_2H + H + M \rightarrow C_2H_2 + M$	$k_0 = 2.64 \cdot 10^{-26} \times e^{-721/T} \times (T/300)^{-3.1}$ $k_\infty = 3.0 \cdot 10^{-10}$	Tsang and Hampson, 1986
83	$C_2H + H_2 \rightarrow C_2H_2 + H$	$5.58 \cdot 10^{-11} \times e^{-1443/T}$	Allen *et al.*, 1992; Stephens *et al.*, 1987
84	$C_2H + O \rightarrow CO + CH$	$1 \cdot 10^{-10} \times e^{-250/T}$	Zahnle, 1986
85	$C_2H + O_2 \rightarrow CO + HCO$	$2 \cdot 10^{-11}$	Brown and Laufer, 1981
86	$C_2H_2 + H + M \rightarrow C_2H_3 + M$	$k_0 = 2.6 \cdot 10^{-31}$ $k_\infty = 8.3 \cdot 10^{-11} \times e^{-1374/T}$	Romani *et al.*, 1993
87	$C_2H_2 + O \rightarrow CH_2^3 + CO$	$2.9 \cdot 10^{-11} \times e^{-1600/T}$	Zahnle, 1986
88	$C_2H_2 + OH + M \rightarrow C_2H_2OH + M$	$k_0 = 5.5 \cdot 10^{-30}$ $k_\infty = 8.3 \cdot 10^{-13} \times (T/300)^{-2}$	Sander *et al.*, 2006
89	$C_2H_2 + OH + M \rightarrow CH_2CO + H + M$	$k_0 = 5.8 \cdot 10^{-31} \times e^{1258/T}$ $k_\infty = 1.4 \cdot 10^{-12} \times e^{388/T}$	Perry and Williamson, 1982
90	$C_2H_2 + OH \rightarrow CO + CH_3$	$2 \cdot 10^{-12} \times e^{-250/T}$	Hampson and Garvin, 1977
91	$C_2H_2OH + H \rightarrow H_2 + CH_2CO$	$3.3 \cdot 10^{-11} \times e^{-2000/T}$	Miller *et al.*, 1982
92	$C_2H_2OH + H \rightarrow H_2O + C_2H_2$	$5 \cdot 10^{-11}$	Miller *et al.*, 1982
93	$C_2H_2OH + O \rightarrow OH + CH_2CO$	$3.3 \cdot 10^{-11} \times e^{-2000/T}$	Miller *et al.*, 1982
94	$C_2H_2OH + OH \rightarrow H_2O + CH_2CO$	$1.7 \cdot 10^{-11} \times e^{-1000/T}$	Miller *et al.*, 1982
95	$C_2H_3 + C_2H_3 \rightarrow C_2H_4 + C_2H_2$	$2.4 \cdot 10^{-11}$	Fahr *et al.*, 1991
96	$C_2H_3 + C_2H_5 \rightarrow C_2H_4 + C_2H_4$	$3 \cdot 10^{-12}$	Laufer *et al.*, 1983
97	$C_2H_3 + C_2H_5 + M \rightarrow CH_3 + C_3H_5 + M$	$k_0 = 1.9 \cdot 10^{-27}$ $k_\infty = 2.5 \cdot 10^{-11}$	Romani *et al.*, 1993
98	$C_2H_3 + C_2H_6 \rightarrow C_2H_4 + C_2H_5$	$3 \cdot 10^{-13} \times e^{-5170/T}$	Kasting *et al.*, 1983
99	$C_2H_3 + CH_3 \rightarrow C_2H_2 + CH_4$	$34 \cdot 10^{-11}$	Fahr *et al.*, 1991
100	$C_2H_3 + CH_3 + M \rightarrow C_3H_6 + M$	$k_0 = 1.3 \cdot 10^{-22}$ $k_\infty = 1.2 \cdot 10^{-10}$	Raymond *et al.*, 2006
101	$C_2H_3 + CH_4 \rightarrow C_2H_4 + CH_3$	$2.4 \cdot 10^{-24} \times e^{-2754/T} \times T^{4.02}$	Tsang and Hampson, 1986
102	$C_2H_3 + H \rightarrow C_2H_2 + H_2$	$3.3 \cdot 10^{-11}$	Warnatz, 1984
103	$C_2H_3 + H_2 \rightarrow C_2H_4 + H$	$2.6 \cdot 10^{-13} \times e^{-2646/T}$	Allen *et al.*, 1992
104	$C_2H_3 + O \rightarrow CH_2CO + H$	$5.5 \cdot 10^{-11}$	Hoyermann *et al.*, 1981
105	$C_2H_3 + OH \rightarrow C_2H_2 + H_2O$	$8.3 \cdot 10^{-12}$	Benson and Haugen, 1967
106	$C_2H_4 + H + M \rightarrow C_2H_5 + M$	$k_0 = 2.15 \cdot 10^{-29} \times e^{-349/T}$ $k_\infty = 4.95 \cdot 10^{-11} \times e^{-1051/T}$	Lightfoot and Pilling, 1987
107	$C_2H_4 + O \rightarrow HCO + CH_3$	$5.5 \cdot 10^{-12} \times e^{-565/T}$	Hampson and Garvin, 1977
108	$C_2H_4 + OH + M \rightarrow C_2H_4OH + M$	$k_0 = 1.0 \cdot 10^{-28} \times (T/300)^{4.5}$ $k_\infty = 8.8 \cdot 10^{-12} \times (T/300)^{0.85}$	Sander *et al.*, 2006
109	$C_2H_4 + OH \rightarrow H_2CO + CH_3$	$2.2 \cdot 10^{-12} \times e^{385/T}$	Hampson and Garvin, 1977
110	$C_2H_4OH + H \rightarrow H_2 + CH_3CHO$	$3.3 \cdot 10^{-11} \times e^{-2000/T}$	Zahnle and Kasting, 1986
111	$C_2H_4OH + H \rightarrow H_2O + C_2H_4$	$5 \cdot 10^{-11}$	Miller *et al.*, 1982

(*continued*)

Table 1. (Continued)

Rxn. #	*Reaction*	*Reaction rate constant*	*Reference*
112	$C_2H_4OH + O \rightarrow OH + CH_3CHO$	$3.3 \cdot 10^{-11} \times e^{-2000/T}$	Zahnle and Kasting, 1986
113	$C_2H_4OH + OH \rightarrow H_2O + CH_3CHO$	$1.7 \cdot 10^{-11} \times e^{-1000/T}$	Zahnle and Kasting, 1986
114	$C_2H_5 + C_2H_3 \rightarrow C_2H_6 + C_2H_2$	$6 \cdot 10^{-12}$	Laufer *et al.*, 1983
115	$C_2H_5 + C_2H_5 \rightarrow C_2H_6 + C_2H_4$	$2.3 \cdot 10^{-12}$	Tsang and Hampson, 1986
116	$C_2H_5 + CH_3 \rightarrow C_2H_4 + CH_4$	$1.88 \cdot 10^{-12} \times (T/300)^{-0.5}$	Romani *et al.*, 1993
117	$C_2H_5 + CH_3 + M \rightarrow C_3H_8 + M$	$k_0 = 3.9 \cdot 10^{-10} \times (T/300)^{2.5}$ $k_\infty = 1.4 \cdot 10^{-8} \times (T/300)^{0.5}$	Romani *et al.*, 1993
118	$C_2H_5 + H \rightarrow C_2H_4 + H_2$	$3 \cdot 10^{-12}$	Tsang and Hampson, 1986
119	$C_2H_5 + H + M \rightarrow C_2H_6 + M$	$k_0 = 5.5 \cdot 10^{-23} \times e^{-1040/T}$ $k_\infty = 1.5 \cdot 10^{-10}$	Gladstone *et al.*, 1996
120	$C_2H_5 + H \rightarrow CH_3 + CH_3$	$7.95 \cdot 10^{-11}$	Gladstone *et al.*, 1996
121	$C_2H_5 + HCO \rightarrow C_2H_6 + CO$	$5 \cdot 10^{-11}$	Pavlov *et al.*, 2001
122	$C_2H_5 + HNO \rightarrow C_2H_6 + NO$	$3 \cdot 10^{-14}$	Pavlov *et al.*, 2001
123	$C_2H_5 + O \rightarrow CH_3 + HCO + H$	$1.1 \cdot 10^{-10}$	Pavlov *et al.*, 2001
124	$C_2H_5 + O \rightarrow CH_3CHO + H$	$1.33 \cdot 10^{-10}$	Tsang and Hampson, 1986
125	$C_2H_5 + O_2 + M \rightarrow CH_3 + HCO + OH + M$	$k_0 = 1.5 \cdot 10^{-28} \times (T/300)^{3.0}$ $k_\infty = 8 \cdot 10^{-12}$	Sander *et al.*, 2006
126	$C_2H_5 + OH \rightarrow CH_3CHO + H_2$	$1 \cdot 10^{-10}$	Pavlov *et al.*, 2001
127	$C_2H_5 + OH \rightarrow C_2H_4 + H_2O$	$4.0 \cdot 10^{-11}$	Pavlov *et al.*, 2001
128	$C_2H_6 + O \rightarrow C_2H_5 + OH$	$8.62 \cdot 10^{-12} \times e^{-2920/T} \times (T/300)^{1.5}$	Baulch *et al.*, 1994
129	$C_2H_6 + O(^1D) \rightarrow C_2H_5 + OH$	$6.29 \cdot 10^{-10}$	Matsumi *et al.*, 1993
130	$C_2H_6 + OH \rightarrow C_2H_5 + H_2O$	$8.54 \cdot 10^{-12} \times e^{-1070/T}$	Sander *et al.*, 2006
131	$C_3H_2 + H + M \rightarrow C_3H_3 + M$	$k_0 = 1.7 \cdot 10^{-26}$ $k_\infty = 1.5 \cdot 10^{-10}$	Yung *et al.*, 1984
132	$C_3H_3 + H + M \rightarrow CH_2CCH_2 + M$	$k_0 = 1.7 \cdot 10^{-26}$ $k_\infty = 1.5 \cdot 10^{-10}$	Yung *et al.*, 1984
133	$C_3H_3 + H + M \rightarrow CH_3C_2H + M$	$k_0 = 1.7 \cdot 10^{-26}$ $k_\infty = 1.5 \cdot 10^{-10}$	Yung *et al.*, 1984
134	$C_3H_5 + CH_3 \rightarrow CH_2CCH_2 + CH_4$	$4.5 \cdot 10^{-12}$	Yung *et al.*, 1984
135	$C_3H_5 + CH_3 \rightarrow CH_3C_2H + CH_4$	$4.5 \cdot 10^{-12}$	Yung *et al.*, 1984
136	$C_3H_5 + H + M \rightarrow C_3H_6 + M$	$k_0 = 1.0 \cdot 10^{-28}$ $k_\infty = 1.0 \cdot 10^{-11}$	Yung *et al.*, 1984
137	$C_3H_5 + H \rightarrow CH_2CCH_2 + H_2$	$1.5 \cdot 10^{-11}$	Yung *et al.*, 1984
138	$C_3H_5 + H \rightarrow CH_3C_2H + H_2$	$1.5 \cdot 10^{-11}$	Yung *et al.*, 1984
139	$C_3H_5 + H \rightarrow CH_4 + C_2H_2$	$1.5 \cdot 10^{-11}$	Yung *et al.*, 1984
140	$C_3H_6 + H + M \rightarrow C_3H_7 + M$	$k_0 = 2.15 \cdot 10^{-29} \times e^{-349/T}$ $k_\infty = 4.95 \cdot 10^{-11} \times e^{-1051/T}$	Pavlov *et al.*, 2001 Assumed same as $k(C_2H_4 + H)$
141	$C_3H_6 + O \rightarrow CH_3 + CH_3CO$	$4.1 \cdot 10^{-12} \times e^{-38/T}$	Hampson and Garvin, 1977
142	$C_3H_6 + OH \rightarrow CH_3CHO + CH_3$	$4.1 \cdot 10^{-12} \times e^{540/T}$	Hampson and Garvin, 1977
143	$C_3H_7 + CH_3 \rightarrow C_3H_6 + CH_4$	$2.5 \cdot 10^{-12} \times e^{-200/T}$	Yung *et al.*, 1984
144	$C_3H_7 + H \rightarrow CH_3 + C_2H_5$	$7.95 \cdot 10^{-11} \times e^{-127/T}$	Pavlov *et al.*, 2001
145	$C_3H_7 + O \rightarrow C_2H_5CHO + H$	$1.1 \cdot 10^{-10}$	Pavlov *et al.*, 2001
146	$C_3H_7 + OH \rightarrow C_2H_5CHO + H_2$	$1.1 \cdot 10^{-10}$	Pavlov *et al.*, 2001
147	$C_3H_8 + O + M \rightarrow C_3H_7 + OH + M$	$k_0 = 1.6 \cdot 10^{-11} \times e^{-2900/T}$ $k_\infty = 2.2 \cdot 10^{-11} \times e^{-2200/T}$	Hampson and Garvin, 1977
148	$C_3H_8 + O(^1D) \rightarrow C_3H_7 + OH$	$1.4 \cdot 10^{-10}$	Pavlov *et al.*, 2001
149	$C_3H_8 + OH \rightarrow C_3H_7 + H_2O$	$8.6 \cdot 10^{-12} \times e^{-615/T}$	Sander *et al.*, 2006
150	$CH + C_2H_2 + M \rightarrow C_3H_2 + H + M$	$k_0 = 2.15 \cdot 10^{-29} \times e^{-349/T}$ $k_\infty = 4.95 \cdot 10^{-11} \times e^{-1051/T}$	Romani *et al.*, 1993
151	$CH + C_2H_4 + M \rightarrow CH_2CCH_2 + H + M$	$k_0 = 1.75 \cdot 10^{-10} \times e^{61/T}$ $k_\infty = 5.3 \cdot 10^{-10}$	Romani *et al.*, 1993
152	$CH + C_2H_4 + M \rightarrow CH_3C_2H + H + M$	$k_0 = 1.75 \cdot 10^{-10} \times e^{61/T}$ $k_\infty = 5.3 \cdot 10^{-10}$	Romani *et al.*, 1993
153	$CH + CH_4 + M \rightarrow C_2H_4 + H + M$	$k_0 = 2.5 \cdot 10^{-11} \times e^{200/T}$ $k_\infty = 1.7 \cdot 10^{-10}$	Romani *et al.*, 1993
154	$CH + CO_2 \rightarrow HCO + CO$	$5.9 \cdot 10^{-12} \times e^{-350/T}$	Berman *et al.*, 1982
155	$CH + H \rightarrow C + H_2$	$1.4 \cdot 10^{-11}$	Becker *et al.*, 1989
156	$CH + H_2 \rightarrow CH_2(^3) + H$	$2.38 \cdot 10^{-10} \times e^{-1760/T}$	Zabarnick *et al.*, 1986
157	$CH + H_2 + M \rightarrow CH_3 + M$	$k_0 = 8.75 \cdot 10^{-31} \times e^{524/T}$ $k_\infty = 8.3 \cdot 10^{-11}$	Romani *et al.*, 1993
158	$CH + O \rightarrow CO + H$	$9.5 \cdot 10^{-11}$	Messing *et al.*, 1981

(*continued*)

Table 1. (Continued)

Rxn. #	*Reaction*	*Reaction rate constant*	*Reference*
159	$CH + O_2 \rightarrow CO + OH$	$5.9 \cdot 10^{-11}$	Butler *et al.*, 1981
160	$CH_2^1 + CH_4 \rightarrow CH_3 + CH_3$	$7.14 \cdot 10^{-12} \times e^{-5050/T}$	Böhland *et al.*, 1985
161	$CH_2^1 + CO_2 \rightarrow H_2CO + CO$	$1 \cdot 10^{-12}$	Zahnle, 1986
162	$CH_2^1 + H_2 \rightarrow CH_2^3 + H_2$	$1.26 \cdot 10^{-11}$	Romani *et al.*, 1993
163	$CH_2^1 + H_2 \rightarrow CH_3 + H$	$5 \cdot 10^{-15}$	Tsang and Hampson, 1986
164	$CH_2^1 + M \rightarrow CH_2^3 + M$	$8.8 \cdot 10^{-12}$	Ashfold *et al.*, 1981
165	$CH_2^1 + O_2 \rightarrow HCO + OH$	$3 \cdot 10^{-11}$	Ashfold *et al.*, 1981
166	$CH_2^3 + C_2H_2 + M \rightarrow CH_2CCH_2 + M$	$k_0 = 3.8 \cdot 10^{-25}$ $k_\infty = 3.7 \cdot 10^{-12}$	Laufer, 1981; Laufer *et al.*, 1983
167	$CH_2^3 + C_2H_2 + M \rightarrow CH_3C_2H + M$	$k_0 = 3.8 \cdot 10^{-25}$ $k_\infty = 2.2 \cdot 10^{-12}$	Laufer, 1981; Laufer *et al.*, 1983
168	$CH_2^3 + C_2H_3 \rightarrow CH_3 + C_2H_2$	$3 \cdot 10^{-11}$	Tsang and Hampson, 1986
169	$CH_2^3 + C_2H_5 \rightarrow CH_3 + C_2H_4$	$3 \cdot 10^{-11}$	Tsang and Hampson, 1986
170	$CH_2^3 + CH_3 \rightarrow C_2H_4 + H$	$7 \cdot 10^{-11}$	Tsang and Hampson, 1986
171	$CH_2^3 + CO + M \rightarrow CH_2CO + M$	$k_0 = 1.0 \cdot 10^{-28}$ $k_\infty = 1.0 \cdot 10^{-15}$	Yung *et al.*, 1984
172	$CH_2^3 + CO_2 \rightarrow H_2CO + CO$	$3.9 \cdot 10^{-14}$	Laufer, 1981
173	$CH_2^3 + H \rightarrow CH + H_2$	$4.7 \cdot 10^{-10} \times e^{-370/T}$	Zabarnick *et al.*, 1986
174	$CH_2^3 + H + M \rightarrow CH_3 + M$	$k_0 = 3.1 \cdot 10^{-30} \times e^{457/T}$ $k_\infty = 1.5 \cdot 10^{-10}$	Gladstone *et al.*, 1996
175	$CH_2^3 + O \rightarrow CH + OH$	$8 \cdot 10^{-12}$	Huebner and Giguere, 1980
176	$CH_2^3 + O \rightarrow CO + HH$	$8.3 \cdot 10^{-11}$	Homann and Wellmann, 1983
177	$CH_2^3 + O \rightarrow HCO + H$	$1 \cdot 10^{-11}$	Huebner and Giguere, 1980
178	$CH_2^3 + O_2 \rightarrow HCO + OH$	$4.1 \cdot 10^{-11} \times e^{-750/T}$	Baulch *et al.*, 1994
179	$CH_2CCH_2 + H \rightarrow C_3H_5$	$k_0 = 8.9 \cdot 10^{-29} \times e^{-1225/T} \times (T/300)^{-2.0}$ $k_\infty = 1.4 \cdot 10^{-11} \times e^{-1000/T}$	Yung *et al.*, 1984
180	$CH_2CCH_2 + H \rightarrow CH_3 + C_2H_2$	$k_0 = 8.9 \cdot 10^{-29} \times e^{-1225/T} \times (T/300)^{-2.0}$ $k_\infty = 9.7 \cdot 10^{-13} \times e^{-1550/T}$	Yung *et al.*, 1984
181	$CH_2CCH_2 + H \rightarrow CH_3C_2H + H$	$1 \cdot 10^{-11} \times e^{-1000/T}$	Yung *et al.*, 1984
182	$CH_2CO + H \rightarrow CH_3 + CO$	$1.9 \cdot 10^{-11} \times e^{-1725/T}$	Michael *et al.*, 1979
183	$CH_2CO + O \rightarrow H_2CO + CO$	$3.3 \cdot 10^{-11}$	Lee, 1980; Miller *et al.*, 1982
184	$CH_3 + C_2H_3 \rightarrow C_3H_5 + H$	$2.4 \cdot 10^{-13}$	Romani *et al.*, 1993
185	$CH_3 + CH_3 + M \rightarrow C_2H_6 + M$	$k_0 = 4.0 \cdot 10^{-24} \times e^{-1390/T} \times (T/300)^{-7.0}$ $k_\infty = 1.79 \cdot 10^{-10} \times e^{-329/T}$	Wagner and Wardlaw, 1988
186	$CH_3 + CO + M \rightarrow CH_3CO + M$	$1.4 \cdot 10^{-32} \times e^{-3000/T} \times den$	Watkins and Word, 1974
187	$CH_3 + H + M \rightarrow CH_4 + M$	$k_0 = 6.0 \cdot 10^{-28} \times (T/298)^{-1.80}$ $k_\infty = 2.0 \cdot 10^{-10} \times (T/298)^{-0.40}$	Baulch *et al.*, 1994; Tsang and Hampson, 1986
188	$CH_3 + H_2CO \rightarrow CH_4 + HCO$	$1.60 \cdot 10^{-16} \times e^{899/T} \times (T/298)^{6.10}$	Baulch *et al.*, 1994
189	$CH_3 + HCO \rightarrow CH_4 + CO$	$2.01 \cdot 10^{-10}$	Tsang and Hampson, 1986
190	$CH_3 + HNO \rightarrow CH_4 + NO$	$1.85 \cdot 10^{-11} \times e^{-176/T} \times (T/298)^{0.6}$	Choi and Lin, 2005
191	$CH_3 + O \rightarrow H_2CO + H$	$1.1 \cdot 10^{-10}$	Sander *et al.*, 2006
192	$CH_3 + O_2 \rightarrow H_2CO + OH$	$k_0 = 4.0 \cdot 10^{-31} \times (T/300)^{-3.6}$ $k_\infty = 1.2 \cdot 10^{-12} \times (T/300)^{-1.1}$	Sander *et al.*, 2006
193	$CH_3 + O_3 \rightarrow H_2CO + HO_2$	$5.4 \cdot 10^{-12} \times e^{-220/T}$	Sander *et al.*, 2006
194	$CH_3 + OH \rightarrow CH_3O + H$	$9.3 \cdot 10^{-11} \times e^{-1606/T} \times (T/298)$	Jasper *et al.*, 2007
195	$CH_3 + OH \rightarrow CO + H_2 + H_2$	$6.7 \cdot 10^{-12}$	Fenimore, 1969
196	$CH_3C_2H + H + M \rightarrow C_3H_5 + M$	$k_0 = 8.88 \cdot 10^{-29} \times e^{-1225/T} \times (T/300)^{-2}$ $k_\infty = 9.7 \cdot 10^{-12} \times e^{-1550/T}$	Yung *et al.*, 1984
197	$CH_3C_2H + H \rightarrow CH_3 + C_2H_2$	$k_0 = 8.88 \cdot 10^{-29} \times e^{-1225/T} \times (T/300)^{-2}$ $k_\infty = 9.7 \cdot 10^{-12} \times e^{-1550/T}$	Whytock *et al.*, 1976
198	$CH_3CHO + CH_3 \rightarrow CH_3CO + CH_4$	$2.8 \cdot 10^{-11} \times e^{-1540/T}$	Zahnle, 1986
199	$CH_3CHO + H \rightarrow CH_3CO + H_2$	$2.8 \cdot 10^{-11} \times e^{-1540/T}$	Zahnle, 1986
200	$CH_3CHO + O \rightarrow CH_3CO + OH$	$5.8 \cdot 10^{-13}$	Washida, 1981
201	$CH_3CHO + OH \rightarrow CH_3CO + H_2O$	$1.6 \cdot 10^{-11}$	Niki *et al.*, 1978
202	$CH_3CO + CH_3 \rightarrow C_2H_6 + CO$	$5.4 \cdot 10^{-11}$	Adachi *et al.*, 1981
203	$CH_3CO + CH_3 \rightarrow CH_4 + CH_2CO$	$8.6 \cdot 10^{-11}$	Adachi *et al.*, 1981
204	$CH_3CO + H \rightarrow CH_4 + CO$	$1 \cdot 10^{-10}$	Zahnle, 1986
205	$CH_3CO + O \rightarrow H_2CO + HCO$	$5 \cdot 10^{-11}$	Zahnle, 1986
206	$CH_3O + CO \rightarrow CH_3 + CO_2$	$2.6 \cdot 10^{-11} \times e^{-5940/T}$	Wen *et al.*, 1989
207	$CH_3O_2 + H \rightarrow CH_4 + O_2$	$1.6 \cdot 10^{-10}$	Tsang and Hampson, 1986
208	$CH_3O_2 + H \rightarrow H_2O + H_2CO$	$1 \cdot 10^{-11}$	Zahnle *et al.*, 2006

(*continued*)

Table 1. (Continued)

Rxn. #	*Reaction*	*Reaction rate constant*	*Reference*
209	$CH_3O_2 + O \rightarrow H_2CO + HO_2$	$1 \cdot 10^{-11}$	Vaghjiani and Ravishankara, 1990
210	$CH_4 + HS \rightarrow CH_3 + H_2S$	$2.99 \cdot 10^{-31}$	Kerr and Trotman-Dickenson, 1957
211	$CH_4 + O \rightarrow CH_3 + OH$	$8.75 \cdot 10^{-12} \times e^{-4330/T} \times (T/298)^{1.5}$	Tsang and Hampson, 1986
212	$CH_4 + O^1D \rightarrow CH_3 + OH$	$1.28 \cdot 10^{-10}$	Sander *et al.*, 2006
213	$CH_4 + O^1D \rightarrow H_2CO + H_2$	$2.25 \cdot 10^{-11}$	Sander *et al.*, 2006
214	$CH_4 + OH \rightarrow CH_3 + H_2O$	$2.45 \cdot 10^{-12} \times e^{-1775/T}$	Sander *et al.*, 2006
215	$CO + O + M \rightarrow CO_2 + M$	$1.7 \cdot 10^{-33} \times e^{-1515/T} \times den$	Tsang and Hampson, 1986
216	$CO + OH \rightarrow CO_2 + H$	$1.5 \cdot 10^{-13} \times (1 + 0.6 \times den)$	Sander *et al.*, 2006
217	$H + CO + M \rightarrow HCO + M$	$5.29 \cdot 10^{-34} \times e^{-100/T} \times den$	Baulch *et al.*, 1994
218	$H + H + M \rightarrow H_2 + M$	$8.85 \cdot 10^{-33} \times (T/298)^{-0.6} \times den$	Baulch *et al.*, 1994
219	$H + HCO \rightarrow H_2 + CO$	$1.5 \cdot 10^{-10}$	Baulch *et al.*, 1992
220	$H + HNO \rightarrow H_2 + NO$	$3.01 \cdot 10^{-11} \times e^{500/T}$	Tsang and Herron, 1991
221	$H + HO_2 \rightarrow H_2 + O_2$	$6.9 \cdot 10^{-12}$	Sander *et al.*, 2006
222	$H + HO_2 \rightarrow H_2O + O$	$1.62 \cdot 10^{-12}$	Sander *et al.*, 2006
223	$H + HO_2 \rightarrow OH + OH$	$7.29 \cdot 10^{-11}$	Sander *et al.*, 2006
224	$H + NO + M \rightarrow HNO + M$	$2.1 \cdot 10^{-32} \times (T/298)^{1.00} \times den$	Hampson and Garvin, 1977
225	$H + O_2 + M \rightarrow HO_2 + M$	$5.7 \cdot 10^{-32} \times 7.5 \cdot 10^{-11} \times (T/298)^{1.6}$	Sander *et al.*, 2006
226	$H + O_3 \rightarrow OH + O_2$	$1.4 \cdot 10^{-10} \times e^{-470/T}$	Sander *et al.*, 2006
227	$H + OH + M \rightarrow H_2O + M$	$6.8 \cdot 10^{-31} \times (T/300)^{-2} \times den$	McEwan and Phillips, 1975
228	$H + SO + M \rightarrow HSO + M$	$k_0 = 5.7 \cdot 10^{-32} \times (T/298)^{1.6}$ $k_\infty = 7.5 \cdot 10^{-11}$	Kasting, 1990
229	$H_2 + O \rightarrow OH + H$	$1.34 \cdot 10^{-15} \times e^{-1460/T} \times (T/298)^{6.52}$	Robie *et al.*, 1990
230	$H_2 + O^1D \rightarrow OH + H$	$1.1 \cdot 10^{-11}$	Sander *et al.*, 2006
231	$H_2 + OH \rightarrow H_2O + H$	$5.5 \cdot 10^{-12} \times e^{-2000/T}$	Sander *et al.*, 2006
232	$H_2CO + H \rightarrow H_2 + HCO$	$2.14^{-12} \times e^{-1090/T} \times (T/298)^{1.62}$	Baulch *et al.*, 1994
233	$H_2CO + O \rightarrow HCO + OH$	$3.4 \cdot 10^{-11} \times e^{-1600/T}$	Sander *et al.*, 2006
234	$H_2CO + OH \rightarrow H_2O + HCO$	$5.5 \cdot 10^{-12} \times e^{125/T}$	Sander *et al.*, 2006
235	$H_2O + O^1D \rightarrow OH + OH$	$2.2 \cdot 10^{-10}$	Sander *et al.*, 2006
236	$H_2O_2 + O \rightarrow OH + HO_2$	$1.4 \cdot 10^{-12} \times e^{-2000/T}$	Sander *et al.*, 2006
237	$H_2O_2 + OH \rightarrow HO_2 + H_2O$	$2.9 \cdot 10^{-12} \times e^{-160/T}$	Sander *et al.*, 2006
238	$H_2S + H \rightarrow H_2 + HS$	$3.66 \cdot 10^{-12} \times e^{-455/T} \times (T/298)^{1.94}$	Peng *et al.*, 1999
239	$H_2S + O \rightarrow OH + HS$	$9.2 \cdot 10^{-12} \times e^{-1800/T}$	Sander *et al.*, 2006
240	$H_2S + OH \rightarrow H_2O + HS$	$6.0 \cdot 10^{-12} \times e^{-70/T}$	Sander *et al.*, 2006
241	$HCO + H + M \rightarrow CO + M$	$6.0 \cdot 10^{-11} \times e^{-7721/T} \times den$	Krasnoperov *et al.*, 2004
242	$HCO + H_2CO \rightarrow CH_3O + CO$	$3.8 \cdot 10^{-17}$	Wen *et al.*, 1989
243	$HCO + HCO \rightarrow H_2CO + CO$	$3.0 \cdot 10^{-11}$	Tsang and Hampson, 1986
244	$HCO + NO \rightarrow HNO + CO$	$1.2 \cdot 10^{-11}$	Tsang and Hampson, 1986
245	$HCO + O_2 \rightarrow HO_2 + CO$	$5.2 \cdot 10^{-12}$	Sander *et al.*, 2006
246	$HNO + NO + M \rightarrow H + M$	$1.04 \cdot 10^{-6} \times e^{25618/T} \times (T/298)^{-1.61} \times den$	Tsang and Hampson, 1986
247	$HNO_2 + OH \rightarrow H_2O + NO_2$	$1.8 \cdot 10^{-11} \times e^{-390/T}$	Sander *et al.*, 2006
248	$HNO_3 + OH \rightarrow H_2O + NO_2 + O$	$7.2 \cdot 10^{-15} \times e^{-785/T} +$ $(1.9 \cdot 10^{-33} \times e^{725/T} \times den)/$ $(1 + 4.6 \cdot 10^{-16} \times e^{-715/T} \times den)$	Sander *et al.*, 2006
249	$HO_2 + HO_2 \rightarrow H_2O_2 + O_2$	$k_0 = 2.3 \cdot 10^{-13} \times e^{590/T}$ $k_\infty = 1.7 \cdot 10^{-33} \times e^{1000/T}$	Sander *et al.*, 2006
250	$HO_2 + O \rightarrow OH + O_2$	$3.0 \cdot 10^{-11} \times e^{200/T}$	Sander *et al.*, 2006
251	$HO_2 + O_3 \rightarrow OH + O_2 + O_2$	$1.1 \cdot 10^{-14} \times e^{-490/T}$	Sander *et al.*, 2006
252	$HS + H \rightarrow H_2 + S$	$3.0 \cdot 10^{-11}$	Schofield, 1973
253	$HS + H_2CO \rightarrow H_2S + HCO$	$1.7 \cdot 10^{-11} \times e^{-800/T}$	Sander *et al.*, 2006
254	$HS + HCO \rightarrow H_2S + CO$	$5.0 \cdot 10^{-11}$	Kasting, 1990
255	$HS + HO_2 \rightarrow H_2S + O_2$	$1.0 \cdot 10^{-11}$	Stachnik and Molina, 1987
256	$HS + HS \rightarrow H_2S + S$	1.5^{-11}	Schofield, 1973
257	$HS + NO_2 \rightarrow HSO + NO$	$2.9 \cdot 10^{-11} \times e^{240/T}$	Sander *et al.*, 2006
258	$HS + O \rightarrow H + SO$	$1.6 \cdot 10^{-10}$	Sander *et al.*, 2006
259	$HS + O_2 \rightarrow OH + SO$	$4.0 \cdot 10^{-19}$	Sander *et al.*, 2006
260	$HS + O_3 \rightarrow HSO + O_2$	$9.0 \cdot 10^{-12} \times e^{-280/T}$	Sander *et al.*, 2006
261	$HS + S \rightarrow H + S_2$	$2.2 \cdot 10^{-11} \times e^{-120/T}$	Kasting, 1990
262	$HSO + H \rightarrow H_2 + SO$	$6.48 \cdot 10^{-12}$	Sander *et al.*, 2006
263	$HSO + H \rightarrow HS + OH$	$7.29 \cdot 10^{-11}$	Sander *et al.*, 2006
264	$HSO + HS \rightarrow H_2S + SO$	$1 \cdot 10^{-12}$	Kasting, 1990
265	$HSO + NO \rightarrow HNO + SO$	$1.0 \cdot 10^{-15}$	Atkinson *et al.*, 2004
266	$HSO + O \rightarrow OH + SO$	$3.0 \cdot 10^{-11} \times e^{-200/T}$	Kasting, 1990

(*continued*)

Table 1. (Continued)

Rxn. #	*Reaction*	*Reaction rate constant*	*Reference*
267	$HSO + OH \rightarrow H_2O + SO$	$5.2 \cdot 10^{-12}$	Sander *et al.*, 2006
268	$HSO + S \rightarrow HS + SO$	$1 \cdot 10^{-11}$	Kasting, 1990
269	$HSO_3 + H \rightarrow H_2 + SO_3$	$1.0 \cdot 10^{-11}$	Kasting, 1990
270	$HSO_3 + O \rightarrow OH + SO_3$	$1.0 \cdot 10^{-11}$	Kasting, 1990
271	$HSO_3 + O_2 \rightarrow HO_2 + SO_3$	$1.3 \cdot 10^{-12} \times e^{-330/T}$	Sander *et al.*, 2006
272	$HSO_3 + OH \rightarrow H_2O + SO_3$	$1.0 \cdot 10^{-11}$	Kasting, 1990
273	$N + NO \rightarrow N_2 + O$	$2.1 \cdot 10^{-11} \times e^{-100/T}$	Sander *et al.*, 2006
274	$N + O_2 \rightarrow NO + O$	$1.5 \cdot 10^{-12} \times e^{-3600/T}$	Sander *et al.*, 2006
275	$N + OH \rightarrow NO + H$	$3.8 \cdot 10^{-11} \times e^{85/T}$	Atkinson *et al.*, 1989
276	$N_2H_3 + H \rightarrow NH_2 + NH_2$	$2.7 \cdot 10^{-12}$	Gehring *et al.*, 1971
277	$N_2H_3 + N_2H_3 \rightarrow N_2H_4 + N_2 + H_2$	$6 \cdot 10^{-11}$	Kuhn and Atreya, 1979
278	$N_2H_4 + H \rightarrow N_2H_3 + H_2$	$9.9 \cdot 10^{-12} \times e^{-1200/T}$	Stief and Payne, 1976
279	$NH + H + M \rightarrow NH_2 + M$	$(6 \cdot 10^{-30} \times den)/(1 + 3 \cdot 10^{-20} \times den)$	Kasting, 1982
280	$NH + NO \rightarrow N_2 + OH$	$4.9 \cdot 10^{-11}$	Sander *et al.*, 2006
281	$NH + O \rightarrow N + OH$	$1 \cdot 10^{-11}$	Kasting, 1982
282	$NH + O \rightarrow NH_2 + CO$	$1 \cdot 10^{-11}$	Pavlov *et al.*, 2001
283	$NH_2 + H + M \rightarrow NH_3 + M$	$(6 \cdot 10^{-30} \times den)/(1 + 3 \cdot 10^{-20} \times den)$	Gordon *et al.*, 1971
284	$NH_2 + HCO \rightarrow NH_3 + CO$	$1 \cdot 10^{-11}$	Pavlov *et al.*, 2001
285	$NH_2 + NH_2 \rightarrow N_2H_4$	$1 \cdot 10^{-10}$	Gordon *et al.*, 1971
286	$NH_2 + NO \rightarrow N_2 + H_2O$	$3.8 \cdot 10^{-12} \times e^{450/T}$	Sander *et al.*, 2006
287	$NH_2 + O \rightarrow HNO + H$	$5 \cdot 10^{-12}$	Albers *et al.*, 1969
288	$NH_2 + O \rightarrow NH + OH$	$5 \cdot 10^{-12}$	Albers *et al.*, 1969
289	$NH_2^* + H_2 \rightarrow NH_3 + H$	$3 \cdot 10^{-11}$	Kasting, 1982
290	$NH_2^* + M \rightarrow NH_2 + M$	$3 \cdot 10^{-11}$	Kasting, 1982
291	$NH_3 + O^1D \rightarrow NH_2 + OH$	$2.5 \cdot 10^{-10}$	Sander *et al.*, 2006
292	$NH_3 + OH \rightarrow NH_2 + H_2O$	$1.7 \cdot 10^{-12} \times e^{-710/T}$	Sander *et al.*, 2006
293	$NO + HO_2 \rightarrow NO_2 + OH$	$3.5 \cdot 10^{-12} \times e^{250/T}$	Sander *et al.*, 2006
294	$NO + O + M \rightarrow NO_2 + M$	$9 \cdot 10^{-31} \times 3 \cdot 10^{-11} \times (T/298)^{1.5}$	Sander *et al.*, 2006
295	$NO + O_3 \rightarrow NO_2 + O_2$	$2.0 \cdot 10^{-12} \times e^{-1400/T}$	Sander *et al.*, 2006
296	$NO + OH + M \rightarrow HNO_2 + M$	$k_0 = 7 \cdot 10^{-31} \times (T/298)^{2.6}$ $k_\infty = 3.6 \cdot 10^{-11} \times (T/298)^{0.1}$	Sander *et al.*, 2006
297	$NO_2 + H \rightarrow NO + OH$	$4 \cdot 10^{-10} \times e^{-340/T}$	Sander *et al.*, 2006
298	$NO_2 + O \rightarrow NO + O_2$	$5.6 \cdot 10^{-12} \times e^{180/T}$	Sander *et al.*, 2006
299	$NO_2 + OH + M \rightarrow HNO_3 + M$	$k_0 = 2.0 \cdot 10^{-30} \times (T/298)^{3.0}$ $k_\infty = 2.5 \cdot 10^{-11}$	Sander *et al.*, 2006
300	$O + HCO \rightarrow H + CO_2$	$5.0 \cdot 10^{-11}$	Tsang and Hampson, 1986
301	$O + HCO \rightarrow OH + CO$	$1.0 \cdot 10^{-10}$	Hampson and Garvin, 1977
302	$O + HNO \rightarrow OH + NO$	$5.99 \cdot 10^{-11}$	Tsang and Hampson, 1986
303	$O + O + M \rightarrow O_2 + M$	$9.46 \cdot 10^{-34} \times e^{480/T} \times den$	Campbell and Gray, 1973
304	$O + O_2 + M \rightarrow O_3 + M$	$6 \cdot 10^{-34} \times 3 \cdot 10^{-11} \times (T/298)^{2.40}$	Sander *et al.*, 2006
305	$O + O_3 \rightarrow O_2 + O_2$	$8.0 \cdot 10^{-12} \times e^{-2060/T}$	Sander *et al.*, 2006
306	$O^1D + M \rightarrow O + M$	$1.8 \cdot 10^{-11} \times e^{110/T}$	Sander *et al.*, 2006
307	$O^1D + O_2 \rightarrow O + O_2$	$3.2 \cdot 10^{-11} \times e^{70/T}$	Sander *et al.*, 2006
308	$OH + HCO \rightarrow H_2O + CO$	$1.7 \cdot 10^{-10}$	Baulch *et al.*, 1992
309	$OH + HNO \rightarrow H_2O + NO$	$5 \cdot 10^{-11}$	Sun *et al.*, 2001
310	$OH + HO_2 \rightarrow H_2O + O_2$	$4.8 \cdot 10^{-11} \times e^{250/T}$	Sander *et al.*, 2006
311	$OH + O \rightarrow H + O_2$	$2.2 \cdot 10^{-11} \times e^{120/T}$	Sander *et al.*, 2006
312	$OH + O_3 \rightarrow HO_2 + O_2$	$1.6 \cdot 10^{-12} \times e^{-940/T}$	Sander *et al.*, 2006
313	$OH + OH \rightarrow H_2O + O$	$4.2 \cdot 10^{-12} \times e^{-240/T}$	Sander *et al.*, 2006
314	$OH + OH \rightarrow H_2O_2$	$6.9 \cdot 10^{-31} \times 1.5 \cdot 10^{-11} \times (T/298)^{0.80}$	Sander *et al.*, 2006
315	$S + CO_2 \rightarrow SO + CO$	$1.0 \cdot 10^{-20}$	Yung and Demore, 1982
316	$S + HCO \rightarrow HS + CO$	$5.0 \cdot 10^{-11}$	Kasting, 1990
317	$S + HO_2 \rightarrow HS + O_2$	$1.5 \cdot 10^{-11}$	Kasting, 1990
318	$S + HO_2 \rightarrow SO + OH$	$1.5 \cdot 10^{-11}$	Kasting, 1990
319	$S + O_2 \rightarrow SO + O$	$2.3 \cdot 10^{-12}$	Sander *et al.*, 2006
320	$S + O_3 \rightarrow SO + O_2$	$1.2 \cdot 10^{-11}$	Sander *et al.*, 2006
321	$S + OH \rightarrow SO + H$	$6.6 \cdot 10^{-11}$	Sander *et al.*, 2006
322	$S + S + M \rightarrow S_2 + M$	$1.98 \cdot 10^{-33} \times e^{-206/T} \times den$	Du *et al.*, 2008
323	$S + S_2 + M \rightarrow S_3 + M$	$2.8 \cdot 10^{-32} \times den$	Kasting, 1990
324	$S + S_3 + M \rightarrow S_4 + M$	$2.8 \cdot 10^{-31} \times den$	Kasting, 1990
325	$S_2 + O \rightarrow S + SO$	$1.1 \cdot 10^{-11}$	Hills *et al.*, 1987
326	$S_2 + S_2 + M \rightarrow S_4 + M$	$2.8 \cdot 10^{-31} \times den$	Baulch *et al.*, 1976

(*continued*)

Table 1. (Continued)

Rxn. #	*Reaction*	*Reaction rate constant*	*Reference*
327	$S_4 + S_4 + M \rightarrow S_8AER + M$	$2.8 \cdot 10^{-31} \times den$	Kasting, 1990
328	$SO + HCO \rightarrow HSO + CO$	$5.6 \cdot 10^{-12} \times (T/298)^{-0.4}$	Kasting, 1990
329	$SO + HO_2 \rightarrow SO_2 + OH$	$2.8 \cdot 10^{-11}$	Kasting, 1990
330	$SO + NO_2 \rightarrow SO_2 + NO$	$1.4 \cdot 10^{-11}$	Sander *et al.*, 2006
331	$SO + O + M \rightarrow SO_2 + M$	$6.0 \cdot 10^{-31} \times den$	Sander *et al.*, 2006
332	$SO + O_2 \rightarrow O + SO_2$	$2.4 \cdot 10^{-13} \times e^{-2370/T}$	Sander *et al.*, 2006
333	$SO + O_3 \rightarrow SO_2 + O_2$	$4.5 \cdot 10^{-12} \times e^{-1170/T}$	Atkinson *et al.*, 2004
334	$SO + OH \rightarrow SO_2 + H$	$8.6 \cdot 10^{-11}$	Sander *et al.*, 2006
335	$SO + SO \rightarrow SO_2 + S$	$3.5 \cdot 10^{-15}$	Martinez and Herron, 1983
336	$SO_2 + HO_2 \rightarrow SO_3 + OH$	$8.63 \cdot 10^{-16}$	Lloyd, 1974
337	$SO_2 + O + M \rightarrow SO_3 + M$	$k_0 = 1.3 \cdot 10^{-33} \times (T/298)^{-3.6}$ $k_\infty = 1.5 \cdot 10^{-11}$	Sander *et al.*, 2006
338	$SO_2 + OH + M \rightarrow HSO_3 + M$	$k_0 = 3 \cdot 10^{-31} \times (T/298)^{3.3}$ $k_\infty = 1.5 \cdot 10^{-12}$	Sander *et al.*, 2006
339	$SO_2^1 + M \rightarrow SO_2 + M$	$1.0 \cdot 10^{-11}$	Turco *et al.*, 1982
340	$SO_2^1 + M \rightarrow SO_2^3 + M$	$1.0 \cdot 10^{-12}$	Turco *et al.*, 1982
341	$SO_2^1 + O_2 \rightarrow SO_3 + O$	$1.0 \cdot 10^{-16}$	Turco *et al.*, 1982
342	$SO_2^1 + SO_2 \rightarrow SO_3 + SO$	$4.0 \cdot 10^{-12}$	Turco *et al.*, 1982
343	$SO_2^3 + M \rightarrow SO_2 + M$	$1.5 \cdot 10^{-13}$	Turco *et al.*, 1982
344	$SO_2^3 + SO_2 \rightarrow SO_3 + SO$	$7.0 \cdot 10^{-14}$	Turco *et al.*, 1982
345	$SO_3 + H_2O \rightarrow H_2SO_4$	$1.2 \cdot 10^{-15}$	Sander *et al.*, 2006
346	$SO_3 + SO \rightarrow SO_2 + SO_2$	$2.0 \cdot 10^{-15}$	Chung *et al.*, 1975
347	$SO_2^1 + h\nu \rightarrow SO_2 + h\nu$	$2.2 \cdot 10^{+4}$	Turco *et al.*, 1982
348	$SO_2^1 + h\nu \rightarrow SO_2^3 + h\nu$	$1.5 \cdot 10^{+3}$	Turco *et al.*, 1982
349	$SO_2^3 + h\nu \rightarrow SO_2 + h\nu$	$1.13 \cdot 10^{+3}$	Turco *et al.*, 1982
350	$O_2 + h\nu \rightarrow O + O^1D$	$1.51 \cdot 10^{+02}$	
351	$O_2 + h\nu \rightarrow O + O$	$2.90 \cdot 10^{+00}$	
352	$H_2O + h\nu \rightarrow H + OH$	$1.65 \cdot 10^{-01}$	
353	$O_3 + h\nu \rightarrow O_2 + O^1D$	$6.44 \cdot 10^{-04}$	
354	$O_3 + h\nu \rightarrow O_2 + O$	$1.64 \cdot 10^{-04}$	
355	$H_2O_2 + h\nu \rightarrow OH + OH$	$2.79 \cdot 10^{-14}$	
356	$CO_2 + h\nu \rightarrow CO + O$	$2.50 \cdot 10^{+01}$	
357	$H_2CO + h\nu \rightarrow H_2 + CO$	$7.71 \cdot 10^{-01}$	
358	$H_2CO + h\nu \rightarrow HCO + H$	$9.33 \cdot 10^{-01}$	
359	$CO_2 + h\nu \rightarrow CO + O^1D$	$2.73 \cdot 10^{+03}$	
360	$HO_2 + h\nu \rightarrow OH + O$	$0.00 \cdot 10^{+00}$	
361	$CH_4 + h\nu \rightarrow CH_2^1 + H_2$	$1.75 \cdot 10^{+00}$	
362	$C_2H_6 + h\nu \rightarrow CH_2^3 + CH_2^3 + H_2$	0.00	
363	$C_2H_6 + h\nu \rightarrow CH_4 + CH_2^1$	$1.48 \cdot 10^{-05}$	
364	$HNO_2 + h\nu \rightarrow NO + OH$	$8.68 \cdot 10^{-22}$	
365	$HNO_3 + h\nu \rightarrow NO_2 + OH$	$2.74 \cdot 10^{-28}$	
366	$NO + h\nu \rightarrow N + O$	$2.04 \cdot 10^{-10}$	
367	$NO_2 + h\nu \rightarrow NO + O$	$4.40 \cdot 10^{-14}$	
368	$CH_3 + h\nu \rightarrow CH_2^1 + H$	$6.67 \cdot 10^{-04}$	
369	$SO + h\nu \rightarrow S + O$	$0.00 \cdot 10^{+00}$	
370	$SO_2 + h\nu \rightarrow SO + O$	$1.37 \cdot 10^{-10}$	
371	$H_2S + h\nu \rightarrow HS + H$	$1.00 \cdot 10^{-23}$	
372	$SO_2 + h\nu \rightarrow SO_2^1$	$1.52 \cdot 10^{-09}$	
373	$SO_2 + h\nu \rightarrow SO_2^3$	$8.14 \cdot 10^{-13}$	
374	$S_2 + h\nu \rightarrow S + S$	$5.94 \cdot 10^{-42}$	
375	$S_2 + h\nu \rightarrow S_2$	$0.00 \cdot 10^{+00}$	
376	$H_2SO_4 + h\nu \rightarrow SO_2 + OH + OH$	$1.66 \cdot 10^{-13}$	
377	$SO_3 + h\nu \rightarrow SO_2 + O$	$0.00 \cdot 10^{+00}$	
378	$SO_2^1 + h\nu \rightarrow SO_2^3 + h\nu$	$9.70 \cdot 10^{-11}$	
379	$SO_2^1 + h\nu \rightarrow SO_2 + h\nu$	$1.42 \cdot 10^{-09}$	
380	$SO_2^3 + h\nu \rightarrow SO_2 + h\nu$	$9.78 \cdot 10^{-11}$	
381	$HSO + h\nu \rightarrow HS + O$	$7.19 \cdot 10^{-17}$	
382	$S_4 + h\nu \rightarrow S_2 + S_2$	$0.00 \cdot 10^{+00}$	
383	$S_3 + h\nu \rightarrow S_2 + S$	$4.22 \cdot 10^{-72}$	
384	$NH_3 + h\nu \rightarrow NH_2 + H$	$6.00 \cdot 10^{-34}$	
385	$N_2H_4 + h\nu \rightarrow N_2H_3 + H$	$9.75 \cdot 10^{-93}$	
386	$NH + h\nu \rightarrow N + H$	$3.99 \cdot 10^{-35}$	

(*continued*)

Table 1. (Continued)

Rxn. #	*Reaction*	*Reaction rate constant*	*Reference*
387	$NH_2 + h\nu \rightarrow NH + H$	$7.49 \cdot 10^{-37}$	
388	$NH_2 + h\nu \rightarrow NH_2^*$	$3.99 \cdot 10^{-35}$	
389	$NH_2^* + h\nu \rightarrow NH_2 + h\nu$	$3.99 \cdot 10^{-35}$	
390	$C_2H_2 + h\nu \rightarrow C_2H + H$	$5.51 \cdot 10^{-07}$	
391	$C_2H_2 + h\nu \rightarrow C_2 + H_2$	$4.09 \cdot 10^{-07}$	
392	$C_2H_4 + h\nu \rightarrow C_2H_2 + H_2$	$5.51 \cdot 10^{-07}$	
393	$C_3H_8 + h\nu \rightarrow C_3H_6 + H_2$	$1.45 \cdot 10^{-12}$	
394	$C_3H_8 + h\nu \rightarrow C_2H_6 + CH_2^1$	$2.49 \cdot 10^{-13}$	
395	$C_3H_8 + h\nu \rightarrow C_2H_4 + CH_4$	$1.08 \cdot 10^{-12}$	
396	$C_3H_8 + h\nu \rightarrow C_2H_5 + CH_3$	$5.88 \cdot 10^{-13}$	
397	$C_2H_6 + h\nu \rightarrow C_2H_2 + H_2 + H_2$	$1.80 \cdot 10^{-05}$	
398	$C_2H_6 + h\nu \rightarrow C_2H_4 + H + H$	$1.93 \cdot 10^{-05}$	
399	$C_2H_6 + h\nu \rightarrow C_2H_4 + H_2$	$5.29 \cdot 10^{-07}$	
400	$C_2H_6 + h\nu \rightarrow CH_3 + CH_3$	$4.79 \cdot 10^{-06}$	
401	$C_2H_4 + h\nu \rightarrow C_2H_2 + H + H$	$5.29 \cdot 10^{-07}$	
402	$C_3H_6 + h\nu \rightarrow C_2H_2 + CH_3 + H$	$5.26 \cdot 10^{-16}$	
403	$CH_4 + h\nu \rightarrow CH_2^3 + H + H$	$1.42 \cdot 10^{+00}$	
404	$CH_4 + h\nu \rightarrow CH_3 + H$	$2.91 \cdot 10^{+00}$	
405	$CH + h\nu \rightarrow C + H$	$9.52 \cdot 10^{-06}$	
406	$CH_2CO + h\nu \rightarrow CH_2^3 + CO$	$8.21 \cdot 10^{-10}$	
407	$CH_3CHO + h\nu \rightarrow CH_3 + HCO$	$1.14 \cdot 10^{-08}$	
408	$CH_3CHO + h\nu \rightarrow CH_4 + CO$	$1.14 \cdot 10^{-08}$	
409	$C_2H_5CHO + h\nu \rightarrow C_2H_5 + HCO$	$6.42 \cdot 10^{-07}$	
410	$C_3H_3 + h\nu \rightarrow C_3H_2 + H$	$6.88 \cdot 10^{-07}$	
411	$CH_3C_2H + h\nu \rightarrow C_3H_3 + H$	$6.42 \cdot 10^{-07}$	
412	$CH_3C_2H + h\nu \rightarrow C_3H_2 + H_2$	$2.41 \cdot 10^{-07}$	
413	$CH_3C_2H + h\nu \rightarrow CH_3 + C_2H$	$3.21 \cdot 10^{-08}$	
414	$CH_2CCH_2 + h\nu \rightarrow C_3H_3 + H$	$6.49 \cdot 10^{-13}$	
415	$CH_2CCH_2 + h\nu \rightarrow C_3H_2 + H_2$	$2.43 \cdot 10^{-13}$	
416	$CH_2CCH_2 + h\nu \rightarrow C_2H_2 + CH_2^3$	$9.73 \cdot 10^{-14}$	
417	$C_3H_6 + h\nu \rightarrow CH_2CCH_2 + H_2$	$8.81 \cdot 10^{-16}$	
418	$C_3H_6 + h\nu \rightarrow C_2H_4 + CH_2^3$	$3.09 \cdot 10^{-17}$	
419	$C_3H_6 + h\nu \rightarrow C_2H + CH_4 + H$	$1.43 \cdot 10^{-10}$	
420	$OCS + h\nu \rightarrow CO + S$	$2.67 \cdot 10^{-36}$	
421	$CS_2 + h\nu \rightarrow CS + S$	$5.40 \cdot 10^{-47}$	
422	$CH_3SH + h\nu \rightarrow H + CH_3S$	$1.48 \cdot 10^{-30}$	
423	$CH_3SH + h\nu \rightarrow HS + CH_3$	$1.11 \cdot 10^{-31}$	
424	$C_2H_6S + h\nu \rightarrow CH_3S + CH_3$	$4.01 \cdot 10^{-93}$	
425	$C_2H_6S_2 + h\nu \rightarrow CH_3S + CH_3S$	$1.65 \cdot 10^{-34}$	
426	$CS_2 + h\nu \rightarrow CS_2^*$	$6.57 \cdot 10^{-48}$	

For photolysis reactions (bottom of table), the "Reaction rate constant" column shows the reaction rate (not the rate constant) at the top of the atmosphere during our "standard" simulation, the modern-day fluxes of CH_4, H_2S, and the S_{org} species on a planet orbiting the Sun. For more on how to calculate reaction rates, see Sander *et al.* (2006).

O_2/O_3 should not be taken as evidence that life does not exist on a planet's surface.

Furthermore, some planets and biospheres will not exhibit the more general feature of photochemical disequilibrium previously proposed as a universal biosignature (Lederberg, 1965; Lovelock, 1965; Des Marais *et al.,* 2002). Unlike Earth's modern-day ecosystem, global anoxic ecosystems may drive an atmosphere toward equilibrium. For example, in the anoxic Archean biospheres considered by Kharecha *et al.* (2005), methanogens and acetogens combine H_2 and CO with CO_2 and H_2O to produce CH_4. They can make a metabolic living by doing this because CH_4 has a lower Gibbs free energy and hence is thermodynamically stable in such a system. The biogenic gases released from such a biosphere result from a drive toward equilibrium, not disequilibrium. Because cases like these could complicate interpretation, it is important to identify additional biosignature gases that might be signs of anoxic biospheres. In this paper, we test the ability of various gases with carbon-sulfur bonds to act as remotely detectable biosignatures for anoxic, inhabited surface environments.

The biosignature potential of S-bearing gases was reviewed by Pilcher (2003), who focused on gases with bonds between methyl groups ($-CH_3$) and sulfur: methanethiol (CH_3SH, also known as methyl mercaptan), dimethyl sulfide (CH_3SCH_3 or DMS), and dimethyl disulfide ($CH_3S_2CH_3$ or DMDS). More recently, Vance *et al.* (2011) suggested that CH_3SH could be used as an *in situ* signature for life on Mars. On modern Earth, the production of these species is dominated by biota, but they are rapidly destroyed by photolysis and by reaction with hydroxyl (OH) radicals (Kettle *et al.,* 2001), and do not build up to concentrations detectable across interstellar distances. In this work, we consider these gases, along with carbon disulfide (CS_2) and carbonyl sulfide (OCS, sometimes abbreviated in other work as COS), two

other biogenic gases that contain carbon-sulfur bonds. These two species—particularly OCS—also have volcanic and photochemical sources, but they are far smaller than biological fluxes. We henceforth use the term "S_{org}" as shorthand to refer to the entire suite of biologically produced species with carbon-sulfur bonds (DMS, DMDS, CH_3SH, CS_2, and OCS). Although hydrogen sulfide (H_2S) is another S-bearing gas produced by biota, large quantities of this species enter the atmosphere via volcanism. Thus, we do not consider it here as a biosignature. However, we do consider the possibility that volcanic H_2S could act as a "false positive" for biogenic S_{org}, as this abiotic H_2S could react in the atmosphere to form S_{org} species. Other work has explored the spectral signatures of sulfur dioxide (SO_2) and H_2S in detail (Kaltenegger and Sasselov, 2010), so we limit our discussion to their potential to be false positives for biological S_{org} production. No study to date has predicted the concentrations of all the S_{org} species in an anoxic atmosphere, nor has any study predicted the spectral features associated with these gases. We used a photochemical model to calculate vertical profiles of these gases for a variety of astronomical and biological contexts, and used a radiative transfer model to predict the spectral features consistent with those profiles.

2. Methods

2.1. Photochemical code

We modified the one-dimensional (altitude), low-O_2 photochemical code originally developed by Kasting *et al.* (1979) to study the anoxic early Earth. The numerics of this model are described by Kasting and Ackerman (1985), and the chemistry was most recently modified by Pavlov *et al.* (2001). We have updated this code, adding seven long-lived chemical species that have lifetimes longer than the time scale for vertical mixing: CH_3SH, DMS, DMDS, OCS, CS_2, methylthiol (CH_3S), and carbon monosulfide (CS). We also added three short-lived species, which are solved in photochemical equilibrium without considering vertical transport: excited-state CS_2, OCS_2, and HCS. These 10 species were incorporated into the chemical scheme by adding 73 chemical reactions. The current model contains 83 chemical species, 46 of which are long lived, connected by 433 chemical reactions. Additionally, many of the 360 reactions from prior work have updated reaction rate constants. A complete list of model reactions, reaction rate constants, and references can be found in Table 1.

The model grid is composed of 100 plane-parallel layers that are each 1 km thick in altitude. We did not perform climate calculations for this work; instead, we assumed a temperature profile for an aerosol-free, ozone-free atmosphere. This profile had a surface temperature of 278 K that decreased to 180 K at the tropopause and was isothermal through the stratosphere. The relatively low surface temperature was picked for consistency with previous Archean photochemistry and climate models (Haqq-Misra *et al.*, 2008), and the isothermal stratosphere is consistent with the model's lack of O_3. The code calculates the mixing ratios of each species in each layer by solving the coupled mass-continuity/flux equations with the reverse Euler method (appropriate for stiff systems) and a variable time-stepping algorithm. For further details on the photochemical code, see Pavlov *et al.* (2001) and references therein.

Unless otherwise stated, all model runs were for a 1-bar, N_2-dominated atmosphere with 3% CO_2 (30,000 ppmv, or $\sim$100 times the present level of CO_2 in Earth's atmosphere) and CH_4/CO_2 ratios < 0.1. These boundary conditions prevent formation of a significant organic haze (Pavlov *et al.*, 2001; Trainer *et al.*, 2006; Domagal-Goldman *et al.*, 2008). These concentrations and the model's other chemical boundary conditions are by no means unique; however, they were chosen for consistency with a methanogen-acetogen ecosystem (Kharecha *et al.*, 2005). The modeling of haze-free atmospheres is, from a photochemical standpoint, conservative. Including haze in the model would shield the gases we are studying from UV radiation and thereby increase their mixing ratios.

2.2. Boundary conditions

At the top of the atmosphere we allowed H and H_2 to escape at the diffusion-limited rate (Walker, 1977). We also applied a constant downward flux of CO and O at the top of our model atmosphere. This accounts for CO and O that is produced from CO_2 photolysis above the top layer of our atmosphere and subsequently flows downward into the model grid. For all other species, we used a zero-flux boundary condition at the top of the atmosphere (*i.e.*, no escape).

At the bottom of the atmosphere, we used constant deposition velocities (to account for reactions with surface rocks and for dissolution in the ocean) for all species except the S_{org} species, CH_4, and NH_3. In addition to constant deposition velocities, H_2S, SO_2, and H_2 had volcanic fluxes of 1×10^9 molecules/cm^2/s, 1×10^{10} molecules/cm^2/s, and 3×10^{10} molecules/cm^2/s, respectively, consistent with past models of Archean Earth (Zahnle *et al.*, 2006) that assume volcanism rates about 3 times modern-day values. These fluxes were distributed throughout the troposphere to simulate volcanism. CH_4 was modeled with a constant flux of 200 Tg C/year (7×10^{10} molecules/cm^2/s) into the bottom layer of the atmosphere, in line with estimates of modern-day non-anthropogenic fluxes on Earth (Intergovernmental Panel on Climate Change, 2007). [The total CH_4 flux today is about 2 times higher; see the Intergovernmental Panel on Climate Change (2007)]. Despite this modern-day flux, the concentrations of CH_4 in our models were much higher than they are today because the lack of atmospheric O_2 allowed CH_4 to accumulate. We imposed a constant mixing ratio of 10^{-10} for NH_3. The corresponding surface flux needed to maintain this mixing ratio was 12.4 Tg N/year, slightly larger than the present-day non-anthropogenic NH_3 flux, 10.5 Tg N/year (Intergovernmental Panel on Climate Change, 2007). All photochemical boundary conditions are listed in Table 2.

We parameterized the biological production of S_{org}. The modern-day S_{org} fluxes, predominantly biological in source, are as follows (in units of molecules/cm^2/s): 0 for DMDS, 4.2×10^9 for DMS, 0 for CH_3S, 8.3×10^8 for CH_3SH, 1.4×10^7 for CS_2, 1.4×10^7 for OCS, and 0 for CS (Kettle *et al.*, 2001). We will use "MDF" as a unit to represent these modern-day fluxes in the rest of this paper, such that 1 MDF S_{org} is equivalent to an atmosphere that receives all S_{org} species at the above fluxes. DMDS, CH_3S, and CS have zero direct biological production but are produced photochemically from

Table 2. A List of Species in Our Photochemical Code along with the Lower Boundary Condition Type and Values, the Latter Given in cgs Units: cm/s for Deposition Velocity (V_{dep}), Dimensionless Mixing Ratio by Volume for Fixed Concentration (f_0), and Molecules/cm^2/s for Flux (flux)

Species	*Lower boundary type*	$V_{dep}/f_0/flux$
O	constant deposition velocity	1
O_2	constant deposition velocity	$1\cdot10^{-04}$
H_2O	constant deposition velocity	0
H	constant deposition velocity	1
OH	constant deposition velocity	1
HO_2	constant deposition velocity	1
H_2O_2	constant deposition velocity	$2\cdot10^{-01}$
H_2	constant deposition velocity*	$2.4\cdot10^{-04}$
CO	constant deposition velocity	$1.2\cdot10^{-04}$
HCO	constant deposition velocity	1
H_2CO	constant deposition velocity	$2\cdot10^{-01}$
CH_4	constant flux	$7\cdot10^{+10}$
CH_3	constant deposition velocity	1
C_2H_6	constant deposition velocity	0
NO	constant deposition velocity	$3\cdot10^{-04}$
NO_2	constant deposition velocity	$3\cdot10^{-03}$
HNO	constant deposition velocity	1
H_2S	constant deposition velocity*	$2\cdot10^{-02}$
HS	constant deposition velocity	1
S	constant deposition velocity	1
SO	constant deposition velocity	$3\cdot10^{-04}$
SO_2	constant deposition velocity*	1
H_2SO_4	constant deposition velocity	1
HSO	constant deposition velocity	1
S_2	constant deposition velocity	0
NH_3	constant mixing ratio	$1\cdot10^{-10}$
NH_2	constant deposition velocity	1
N_2H_3	constant deposition velocity	1
N_2H_4	constant deposition velocity	$2\cdot10^{-01}$
CH_2^3	constant deposition velocity	0
C_2H_5	constant deposition velocity	0
C_2H_2	constant deposition velocity	0
C_2H_4	constant deposition velocity	0
C_3H_8	constant deposition velocity	0
C_2H_3	constant deposition velocity	0
C_3H_6	constant deposition velocity	0
C_3H_2	constant deposition velocity	0
CH_2CCH_2	constant deposition velocity	0
CH_3C_2H	constant deposition velocity	0
$C_2H_6S_2$ (DMDS)	constant flux	0
C_2H_6S (DMS)	constant flux	$4.20\cdot10^{+09}$
CH_3S	constant deposition velocity	$1\cdot10^{-02}$
CH_3SH	constant flux	$8.3\cdot10^{+08}$
CS_2	constant flux	$1.4\cdot10^{+07}$
OCS	constant flux	$1.4\cdot10^{+07}$
CS	constant deposition velocity	$1\cdot10^{-04}$

*In addition to a constant deposition velocity, we also use a volcanic flux for these gases. Specifically, we used volcanic fluxes of $3\cdot10^{10}$ molecules/cm^2/s of H_2, $1\cdot10^{10}$ molecules/cm^2/s of SO_2, and $1\cdot10^{9}$ molecules/cm^2/s of H_2S.

other S_{org} species and are needed to ensure a comprehensive modeling of S_{org} chemistry. To determine the effect of S_{org} fluxes on S_{org} mixing ratios and ultimately on disc-averaged planetary spectra, we parameterized S_{org} flux rates by holding the ratios of these fluxes constant and multiplying each flux by a common factor.

Most S_{org} species are produced via methylation of (addition of methyl groups to) CH_3SH or dehydrogenation of (removal of H atoms from) CH_3SH, or both. The main modern-day global source of CH_3SH is the degradation of methionine, an amino acid that contains a terminal methio group ($-SCH_3$), from eukaryotes. Based on the production rate of methionine, Pilcher (2003) estimated the flux of CH_3SH during the Archean to be $\sim3\times10^9$ mol/year, or about 0.01 MDF CH_3SH. This estimate agrees with what one would get by simply scaling CH_3SH production linearly with net primary productivity, as that is also estimated to have been ~0.01 times the modern value (Kharecha *et al.,* 2005). Because the Archean is our lone example of an anoxic planet, Pilcher's work serves as an estimate for the S_{org} fluxes on extrasolar planets with anoxic surface conditions. However, these fluxes could vary if methionine (or some other S-containing amino acid) was more or less prevalent in the planet's biota or if the biospheric productivity was different. Thus, in our primary suite of model runs, we parameterize the S_{org} fluxes from methionine degradation, using values from 0 to 3000 times those estimated by Pilcher (2003) (this is equivalent to 0–30 MDF S_{org}).

The direct production of CH_3SH for metabolic purposes could lead to higher S_{org} fluxes. *Methanosarcina acetivorans,* a methanogen, can produce CH_3SH via the metabolic reaction $3CO+H_2S+H_2O\rightarrow CH_3SH+2CO_2$ (Moran *et al.,* 2008). In the rest of this manuscript, we will refer to this metabolism as "mercaptogenesis" and to the organisms that utilize it as "mercaptogens." Assuming substrate-limited (CO-/H_2S-limited) conditions with no competition for substrates places an upper limit on mercaptogenesis. CO should build up to extremely high levels on planets with anoxic atmospheres unless consumed by biota (Zahnle, 1986; Kharecha *et al.,* 2005); thus, H_2S is likely the limiting substrate on such planets. Estimates of the net primary productivity of S-consumers on Archean Earth vary by orders of magnitude, from 5×10^9 mol S/year (Kharecha *et al.,* 2005) to 2×10^{14} mol S/year (Canfield, 2005). Both estimates have caveats: the lower estimate did not include a complete S cycle that allowed for recycling of S, and the upper estimate neglected inorganic sinks for S such as metal-sulfide deposition. The former omission likely has a larger impact, so we used Canfield's estimate as an upper limit to S utilization. If mercaptogens accounted for all H_2S used by metabolism, the range of the above S consumption estimates would correspond to CH_3SH fluxes of $\sim3\times10^9$ to 1×10^{14} moles CH_3SH/year, or 0.03–1000 MDF CH_3SH. Thus, 1000 MDF CH_3SH is an upper limit to the CH_3SH produced by mercaptogens on early Earth. The actual CH_3SH production was likely much lower than this, due to competition for CO and H_2S from other metabolisms or from scavenging of S from the oceans by metal precipitates. On an extrasolar planet, the CH_3SH production rate could be higher if the planet has larger volcanic H_2S flux rates. Constraining such fluxes may be possible via absorption features of volcanic gases in planetary spectra (Kaltenegger *et al.,* 2010).

Unfortunately, no anoxic ocean model currently exists that includes biological S recycling and a complete accounting of oceanic S sources. Furthermore, no code exists that can model mercaptogens in the context of CO-consuming methanogens and sulfur oxidizers that could compete for substrates. These problems might eventually be addressed by the development

of ocean biogeochemistry codes with flexible chemistries and a wide variety of metabolisms. In the absence of such codes, we parameterized CH_3SH fluxes from 1 to 100 MDF to simulate a biosphere with CO-consuming mercaptogens. Because the CO they consume would otherwise be used by methanogens, we decreased the biological CH_4 flux in proportion to the biological CH_3SH flux in these simulations. In this set of mercaptogenesis experiments with 1–100 MDF CH_3SH, we held the fluxes of the other S_{org} gases (DMS, DMDS, OCS, and CS_2) constant at 1 MDF, because, unlike CH_3SH, these gases are not directly produced by this metabolism. To distinguish between the two sets of experiments, we label model simulations where we changed the flux of all S_{org} gases with "X MDF S_{org}," and label model simulations where we changed only the flux of CH_3SH with "X MDF CH_3SH."

Each set of S_{org} boundary conditions was applied to planets orbiting stars of three different spectral types, following Segura *et al.* (2005). Specifically, we used time-averaged spectra of the Sun, the active M dwarf AD Leo, and a model-generated M dwarf with a surface temperature of 3100 K and no chromosphere (Allard *et al.,* 1997). This star, referred to as "T3100" in the remainder of this manuscript, is not presented as a physically meaningful case but rather as a low-UV-flux, end-member simulation. All stellar spectra were scaled such that the total energy flux at the top of the model planet's atmosphere was $1092\,W/m^2$, including radiation outside the bounds of our photochemical model wavelength grid. This is 80% of the flux Earth currently receives from the Sun, which is in line with the amount of energy the anoxic, Archean Earth received. Because the total energy flux received by the planet is the same, this is equivalent to assuming that the planet orbits within the habitable zone of that star. The resulting scaled stellar spectra are plotted in Fig. 1, as binned for use in the photochemical code.

2.3. Radiative transfer code

We used the line-by-line Spectral Mapping Atmospheric Radiative Transfer model (Meadows and Crisp, 1996; Crisp, 1997) to generate synthetic planetary spectra of our model planets. Spectra were computed by using the vertical mixing ratio profiles of CH_3SH, DMS, DMDS, OCS, CS_2, SO_2, H_2S, CH_4, C_2H_6, CO_2, and H_2O generated by the photochemical code. The underlying surface consisted of a 278 K global ocean with an emissivity of $\sim$1, and we used the same assumed temperature structure applied in the photochemical model. The input stellar spectra and molecular absorption data were obtained from the Virtual Planetary Laboratory's online database (http://vpl.astro.washington.edu/spectra/VPLSpectra/frontpage.htm) and include molecular line parameters from the HITRAN (Rothman *et al.,* 2005) and PNNL databases (Sharpe *et al.,* 2004).

We did not include any aerosols in our spectral model, so the model spectra shown here should be considered idealized "clear sky" simulations. However, we limited parameter space (see Boundary conditions, above) so that the atmospheric CH_4/CO_2 ratio was less than 0.1, a condition for which thick organic haze layers will not form (Trainer *et al.,* 2006; Haqq-Misra *et al.,* 2008). S_8 and sulfate hazes were also limited by these conditions. Assuming Mie scattering, all S_8, hydrocarbon, and sulfate particles in our simulations had extinction optical depths less than 0.05 within the "IR window" between 8.5 and 13 μm in which most of the absorption features explored here appear. While organo-sulfate particles can form in sulfur-rich anoxic atmospheres (DeWitt *et al.,* 2010), the optical properties of these particles have not yet been explored. Water clouds may also impact the spectra simulated here. For more on the effects of water clouds, see Robinson *et al.* (2011). We leave the exploration of aerosol and cloud effects for future studies.

3. Results

The habitable-zone planets around stars with lower surface temperatures receive proportionally fewer UV photons and more long-wavelength, low-energy photons (Fig. 1). This leads to lower photolysis rates on these planets, as there are fewer photons with the requisite energy to dissociate molecules. Figure 1b illustrates this by showing the wavelength-dependent absorption cross section for CH_3SH (Sharpe *et al.,* 2004), along with the incident UV flux from the three different stars. Photolysis of CH_3SH (and the other S_{org} species) generally occurs at wavelengths <300 nm, where the fluxes from the Sun, AD Leo, and T3100 differ by orders of magnitude. Except below 170 nm, where the AD Leo habitable-zone planet receives the highest relative flux, the UV flux decreases dramatically going from the Sun to AD Leo to T3100. Because CH_3SH photolysis occurs mostly in the 200–300 nm region, its photolysis rate follows this same pattern. The same holds true for other gases, for example, H_2O, whose photolysis creates highly reactive radicals that destroy S_{org}.

3.1. Production and loss of S_{org} species

We define a standard Archean model with the general boundary conditions above along with 1 MDF S_{org} and 1 MDF CH_4. The largest S_{org} sinks in this simulation were the following reactions:

$$C_2H_6S_2 + O \rightarrow CH_3 + SO + CH_3S$$
$$OCS + h\nu \rightarrow CO + S$$
$$C_2H_6S + O \rightarrow CH_3 + CH_3 + SO$$
$$CH_3SH + O \rightarrow CH_3 + HSO$$

These reactions outpaced other net S_{org} sinks by at least an order of magnitude. Thus, the major sink for S_{org} in our model was reaction with O, and the major by-products were CH_3 and oxidized sulfur species—SO and HSO. The major source of O atoms to the atmosphere was photolysis of major atmospheric components (in an anoxic atmosphere, CO_2, SO_2, and H_2O), and the inventory of O atoms decreased when the flux of UV photons to the atmosphere was diminished.

On the model planet orbiting T3100, the biggest sinks for S_{org} species were the following reactions:

$$OCS + h\nu \rightarrow CO + S$$
$$OCS + S \rightarrow CO + S_2$$
$$CH_3SH + h\nu \rightarrow CH_3 + HS$$
$$C_2H_6S_2 + O \rightarrow CH_3 + SO + CH_3S$$
$$CH_3SH + O \rightarrow CH_3 + HSO$$

In the model simulations around these stars, the lack of UV photons entering the atmosphere led to a lack of O radicals in

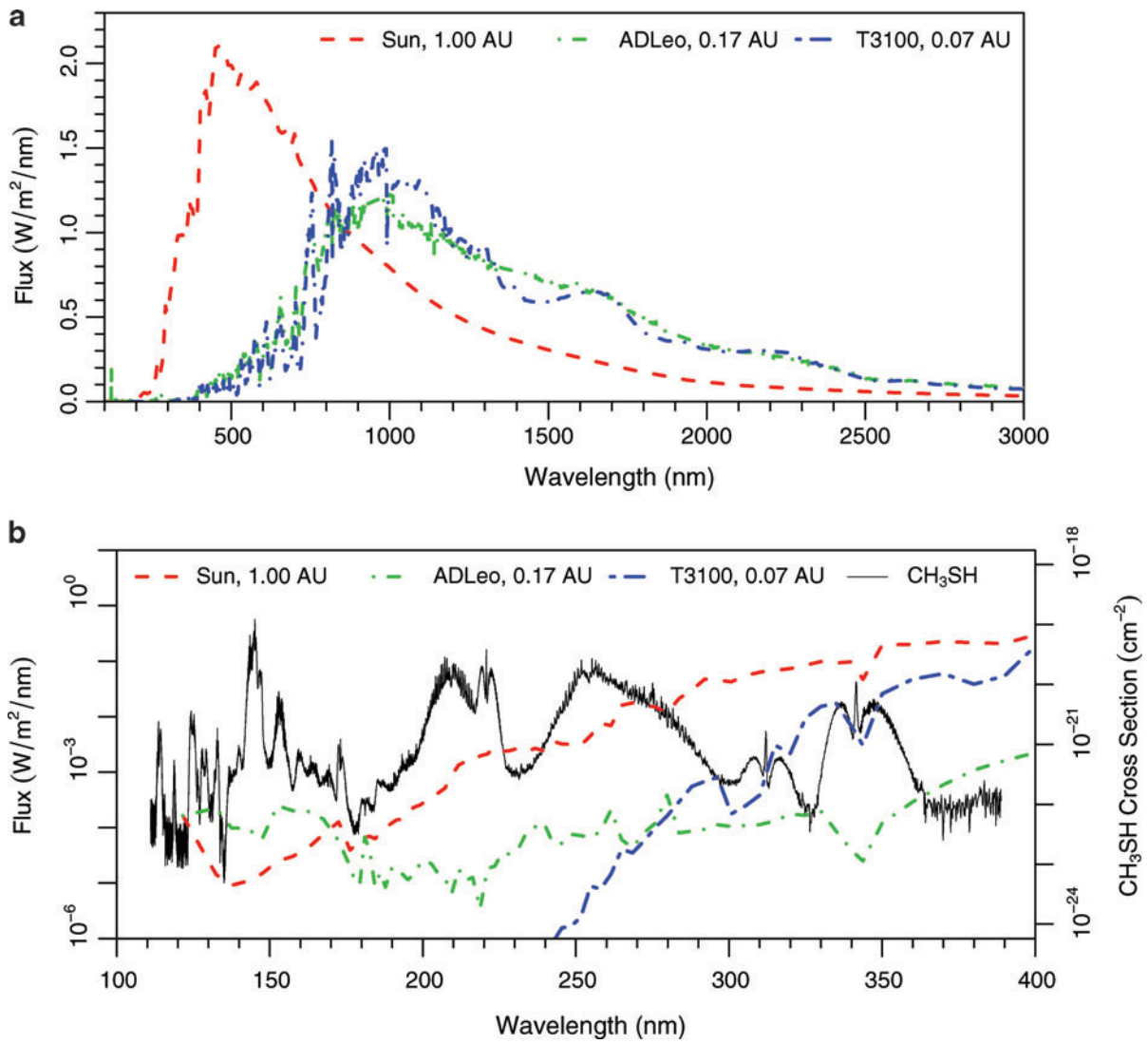

FIG. 1. (**a**) The stellar energy distribution at a planet receiving the same amount of total energy flux that the Earth received ~2.5 billion years ago for three different stars: the Sun, AD Leo, and T3100 (a model M dwarf that has no chromosphere). (**b**) The bottom panel is an expansion of the UV region of the top panel, with a logarithmic *y* axis. The bottom panel also shows the absorption cross section of CH_3SH, units for which are on the right *y* axis (also logarithmic). Color images available online at www.liebertonline.com/ast

the atmosphere. This caused a slower destruction rate of the S_{org} gases and shifted the main by-products of S_{org} photochemistry to carbon monoxide (CO) and reduced sulfur species (S, S_2, and H_2S). The planets orbiting AD Leo were between these two end-member cases for atomic O production. As a result, the by-products of S_{org} chemistry on planets around M dwarfs were a mix of oxidized and reduced sulfur species.

3.2. Atmospheric profiles

Results from nine photochemical model runs are shown in Figs. 2 and 3. Each figure contains a 3×3 grid of panels with decreasing UV flux (Sun, AD Leo, T3100) from left to right and increasing organic sulfur gases (0 MDF S_{org}, our control; 1 MDF S_{org}, the modern-day fluxes; and 10 MDF CH_3SH, corresponding to a biosphere containing mercaptogens) from top to bottom. Figure 2 shows the calculated mixing ratio profiles of the major S_{org} species along with SO_2 and H_2S, while Fig. 3 shows the calculated vertical profiles of H_2O, CH_4, C_2H_6, H_2, and O_2. The profiles generated with 0 MDF S_{org} are our control experiments, as this boundary condition is equivalent to assuming no biological S_{org} production. In these cases, the atmospheric mixing ratios of all S_{org} gases were extremely low.

For models with the modern-day S_{org} flux, near-surface mixing ratios of DMS built up to at least ~10 ppt (10^{-11}) for all three stellar types. These relatively low concentrations are due to higher photolysis rates in the absence of an O_2/O_3 UV shield. For the T3100 model planet, DMDS and CH_3SH peaked above 100 ppb (10^{-7}). The shapes of the S_{org} profiles also changed as a function of star type, as the sulfur gases remained well mixed to higher altitudes in the low-UV-flux models, further increasing the total column depths of the S_{org} species. C_2H_6 concentrations also increased when surface S_{org} production was included, because of additional production of CH_3 radicals (Fig. 3).

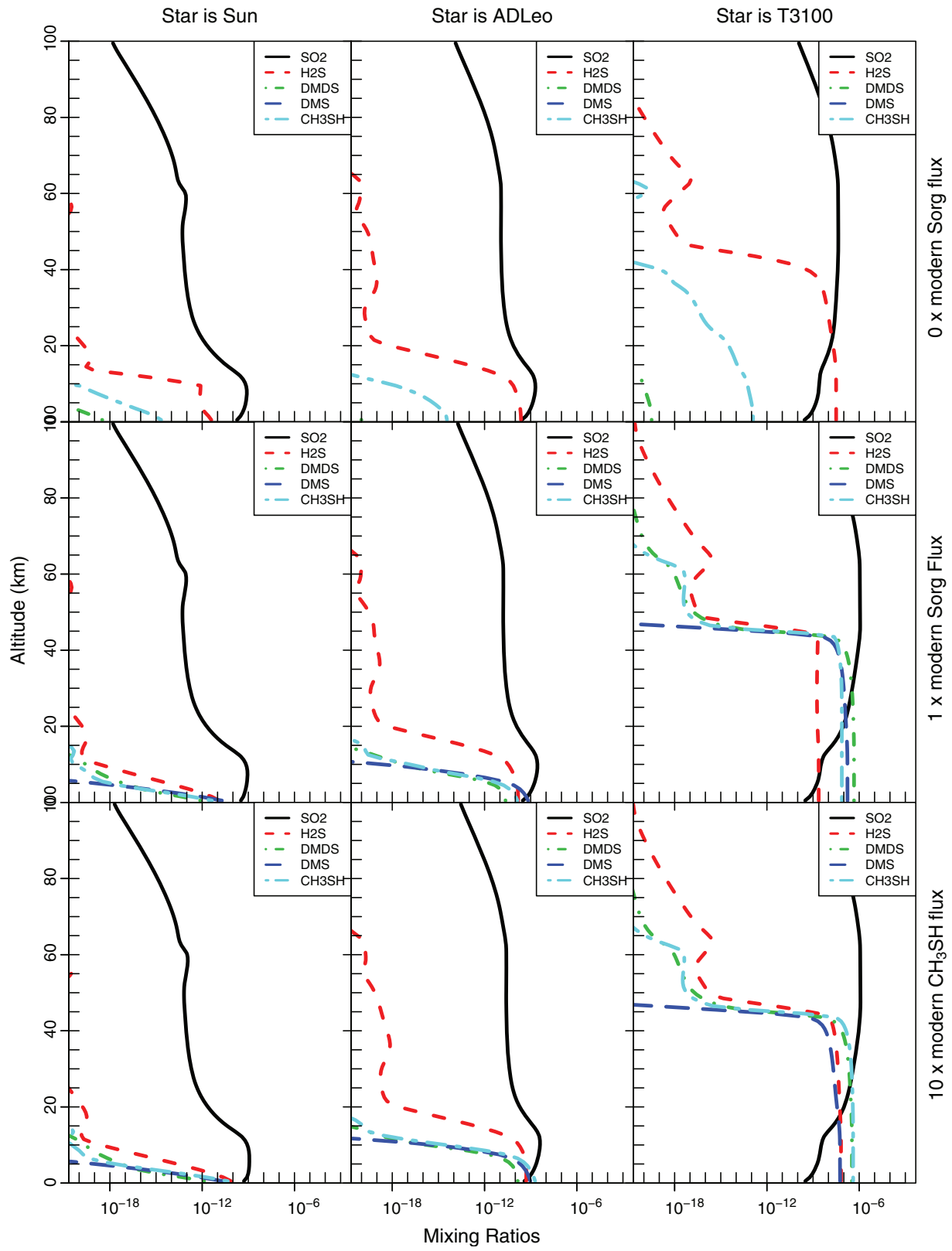

FIG. 2. These nine panels each show model-predicted vertical profiles of the mixing ratios of the organic sulfur species. Panels toward the left are for planets orbiting stars with greater UV radiation, and panels toward the bottom are for planets with higher biological S_{org} production. The S_{org} mixing ratios increase with higher ground S_{org} fluxes (bottom panels) and with lower UV radiation (right panels). Color images available online at www.liebertonline.com/ast

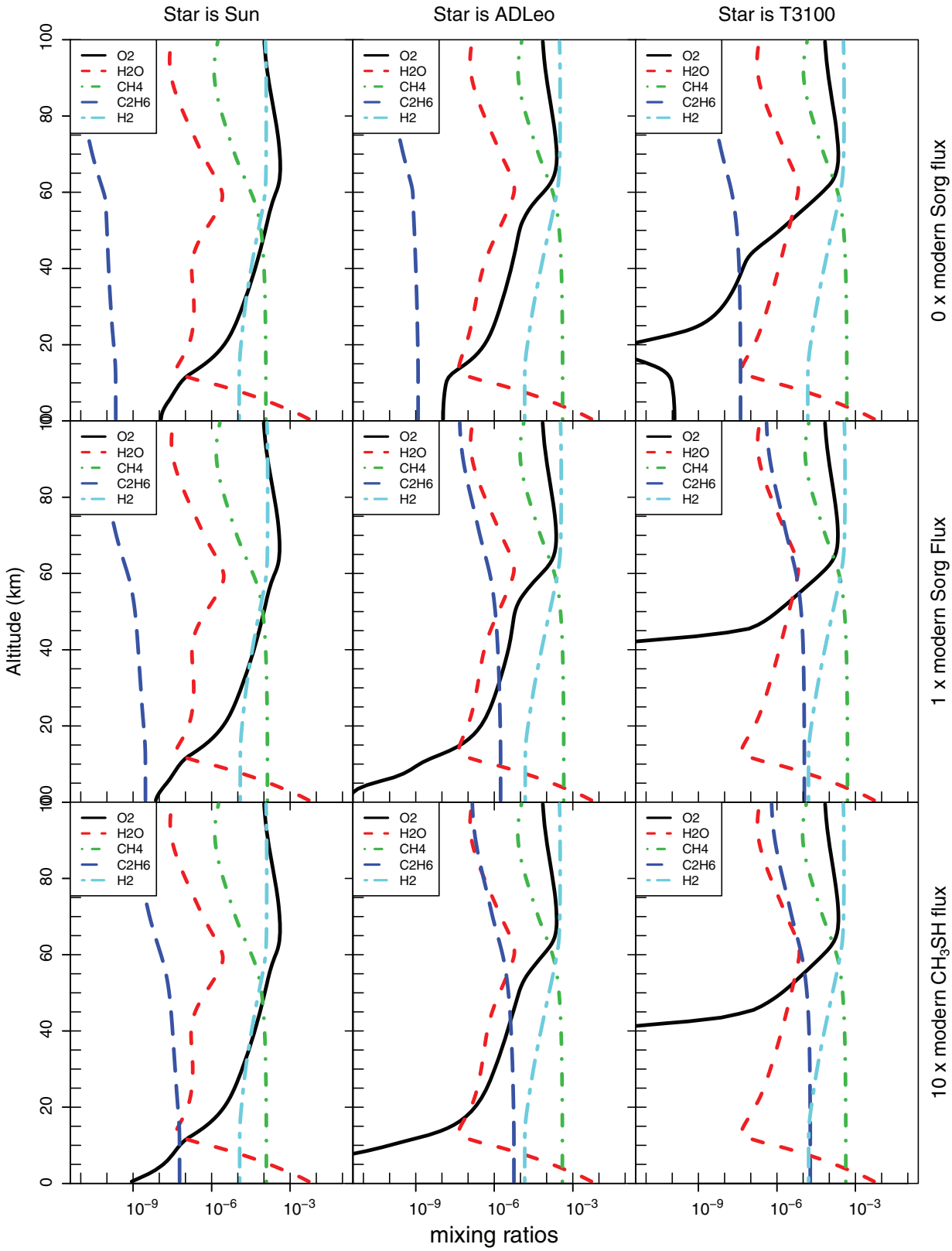

FIG. 3. These nine panels each show model-predicted vertical profiles of the mixing ratios of the greenhouse gases in our climate and line-by-line radiative transfer models. Panels on the left are for planets orbiting stars with greater UV radiation, and panels on the bottom are for planets with higher biological S_{org} production. H_2O and CO_2 concentrations are identical in all model runs, while CH_4 concentrations vary only modestly between simulations. Note the increase in C_2H_6 concentrations on planets with higher S_{org} fluxes or lower UV radiation, or both. Color images available online at www.liebertonline.com/ast

As expected, increasing the CH_3SH flux to 10 MDF while keeping the rest of the S_{org} gases at 1 MDF (the mercaptogen experiments) resulted in a further increase in all S_{org} mixing ratios (Fig. 2). This increase was most pronounced in CH_3SH and in DMDS and was greatest on planets receiving relatively low UV radiation. C_2H_6 concentrations also increased with these higher CH_3SH fluxes (Fig. 3), despite the fact that we decreased the CH_4 fluxes in these simulations so that the total flux of CH_3 groups to the atmosphere remained constant.

3.3. Spectra

To illustrate where each of the gases plotted in Figs. 2 and 3 are spectrally active, we present sensitivity spectra of the model planet with 30 MDF CH_3SH orbiting AD Leo (Fig. 4). We generated Fig. 4 by running a full spectral model (shown as a black curve) and then subsequent model runs with one gas removed in each run. These sensitivity spectra are not self-consistent atmospheres; rather, they are tools to determine what gases are causing certain absorption features in the full spectral model. The spectral regions in which a sensitivity spectrum for a particular gas differs from the planet's complete spectrum show where that gas absorbs. For example, the effects of H_2O are clearly seen (difference between black and gray curves) from 5 to 7 μm and longward of 17 μm. Likewise, CO_2 absorption features (difference between black and brown curves) are present from 9 to 11 μm and from 12 to 19 μm, CH_4 absorption is present from 6 to 9 μm, and C_2H_6 has a deep absorption feature from 11 to 13 μm. The distinguishable S_{org} absorption features include those caused by CH_3SH from 9 to 11 μm and by DMDS from 10 to 11 μm.

Model spectra from 4 to 20 μm are presented at a spectral resolution of R ($\lambda/\Delta\lambda$) $\sim$ 50 in Fig. 5. This resolution is consistent with the requirement goal for the Terrestrial Planet Finder Interferometer (TPF-I), a first-generation thermal-IR planet characterization mission (Lawson *et al.*, 2007). For the simulations of a mercaptogen biosphere on a planet with a spectrum of the Sun or AD Leo, the greatest remotely observable difference was the C_2H_6 absorption feature between 11 and 13 μm, the strength of which increases at higher CH_3SH fluxes (30 $\times$ modern CH_3SH flux). This feature became more prevalent if we increased the flux of the other S_{org} gases (30 $\times$ modern S_{org} flux) or if we decreased the UV radiation reaching the planet (bottom panel). The model simulations with these deeper C_2H_6 features also exhibited enhanced absorption features from 8.5 to 11 μm caused by DMDS.

H_2S fluxes are unlikely to cause false positives. H_2S had a large spectral influence only on planets with extremely large H_2S fluxes (1000 $\times$ H_2S MDF) orbiting stars with extremely low UV radiation (T3100). Except for these end-member cases, we do not expect H_2S to provide a false negative for the other absorption features discussed here.

4. Discussion

Several trends from our photochemical simulations (Figs. 2 and 3) have implications for the interpretation of future exoplanetary spectra. As the stellar UV flux to the planet decreases, the ground-level mixing ratios and altitudinal extent of S_{org} species increase. The same effects can also be caused by increases to the S_{org} surface fluxes. Both trends can be explained by an increase in the ratio of S_{org} sources to S_{org} sinks. The main sources of S_{org} to the atmosphere are the biogenic surface fluxes; an increase in these raises the source/sink ratio. The two main sinks of S_{org} species are direct photolysis and reaction with radicals such as OH and O that themselves are by-products of photochemical reactions. The decrease in UV radiation slows all photolysis and therefore decreases the sinks for S_{org} species.

The other robust trend in the photochemical simulations is an increase in C_2H_6 with increasing S_{org} fluxes and with decreasing UV radiation. Increasing S_{org} fluxes increases the source of CH_3 radicals that combine to form C_2H_6. Decreases in UV fluxes lead to lower C_2H_6 photolysis rates, lower concentrations of C_2H_6-destroying radicals, and smaller sinks for C_2H_6.

C_2H_6 has not previously been identified as a potential biosignature for anoxic atmospheres, although most concepts for mid-IR exoplanet characterization missions already include plans to detect CH_4 by looking for its absorption feature centered near 7.7 μm (Lawson *et al.*, 2007). According to our model simulations, C_2H_6 detection would require an interferometer with a spectral resolution of $\lambda/\Delta\lambda \sim 20$ and a S/N $\sim$ 15 in the 11–13 μm range to resolve the distinctive band profile for this gas. Such a mission could discriminate at a 3σ level between C_2H_6 produced by the model with the modern-day S_{org} flux and the model with no S_{org} flux, for a planet around an M dwarf similar to AD Leo.

C_2H_6 concentrations can be enhanced both by increased S_{org} concentrations and by increased CH_4. Because CH_4 can have an abiogenic source, CH_4-derived C_2H_6 could be abiogenic in origin. Figure 5 shows low-resolution ($R \sim 50$) spectra with high C_2H_6 concentrations arising from either high S_{org} fluxes or high CH_4 fluxes. Models that have higher S_{org} fluxes have higher C_2H_6 concentrations and a deeper C_2H_6 absorption feature between 11 and 13 μm. Similarly, models that have higher CH_4 fluxes also have increased C_2H_6 concentrations and more absorption between 11 and 13 μm. However, models that achieve C_2H_6 buildup through increased CH_4 fluxes also exhibit a detectable increase in the CH_4 concentrations in the atmosphere: there was a doubling in the near-surface CH_4 mixing ratios when the CH_4 fluxes were increased to 1.5 MDF, and another doubling when the CH_4 fluxes were increased to 2.0 MDF. These increased CH_4 concentrations caused significantly more absorption between 8 and 9 μm. In other words, changes in the absorption by CH_4 could potentially allow us to discriminate between the spectra with "abiogenic, CH_4-derived C_2H_6" and the spectra with "biogenic, S_{org}-derived C_2H_6." Thus, an exoplanet characterization mission that can measure the depths of the CH_4 and C_2H_6 absorption features accurately enough to estimate the C_2H_6/CH_4 ratio may be able to determine whether biological S_{org} production contributes to the source of C_2H_6.

These above differences in CH_4 absorption depths in biological and abiological model simulations are the result of higher C_2H_6/CH_4 ratios in models with biological S_{org} fluxes. These fluxes caused an increase in atmospheric CH_3 groups, which in turn increased the atmospheric C_2H_6/CH_4 ratio. Thus, for a given amount of C_2H_6, the CH_4 concentrations were lower in models with higher S_{org} fluxes. (The converse is also true; for a given CH_4 concentration, models with higher S_{org} fluxes exhibited higher C_2H_6 concentrations.) This effect could be augmented by inclusion of other

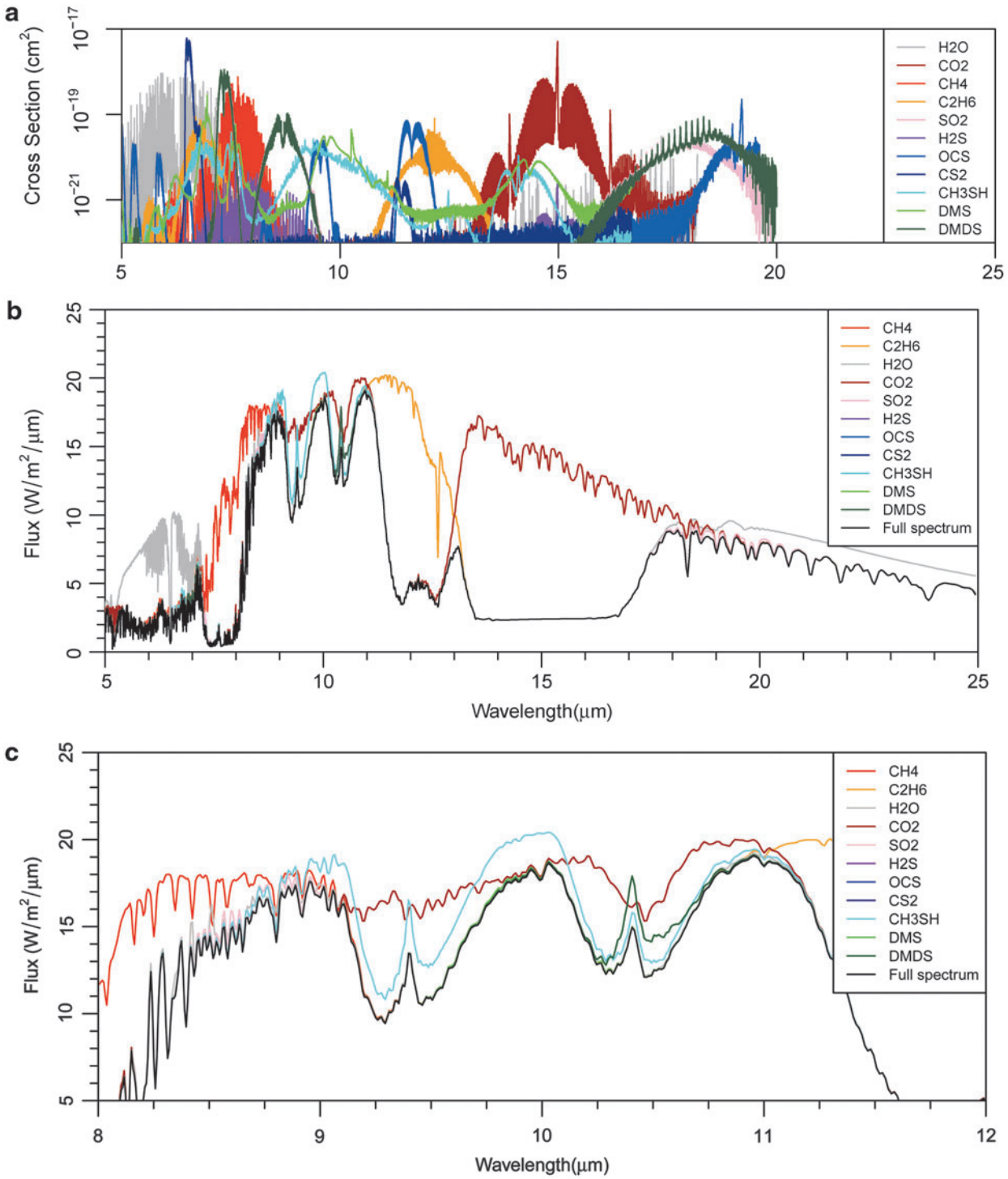

FIG. 4. The top panel shows the absorption cross sections for the gases included in our spectral model. The middle and bottom panels show the simulated spectra for a simulation of a planet with 30 MDF S_{org} orbiting AD Leo. The black line shows the full model spectrum, including the influence of all the gases in our line-by-line radiative transfer model. The colored lines show model spectra in which one gas is removed from the line-by-line radiative transfer model, with lines of the same color showing the absorption cross-section spectrum for that gas in the top pane. For example, the gray line shows the spectrum with the radiative influence of H_2O removed from the model. The bottom panel shows a zoom-in on the "infrared window" between 8.5 and 11 μm.

biological CH_3X species, such as CH_3Cl, that were not included in these simulations.

In addition to the influence of S_{org} species on the C_2H_6 feature, several other features were caused directly by the presence of the S_{org} in the model atmospheres: absorption just shortward of 7 μm by DMS, absorption just longward of 7 μm by DMDS, absorption from 8.5 to 9.5 μm by DMDS, and absorption between 9 and 11 μm by DMDS and CH_3SH. When present, these features created a continuous, but not constant, increase in absorption from 6 μm all the way to the C_2H_6

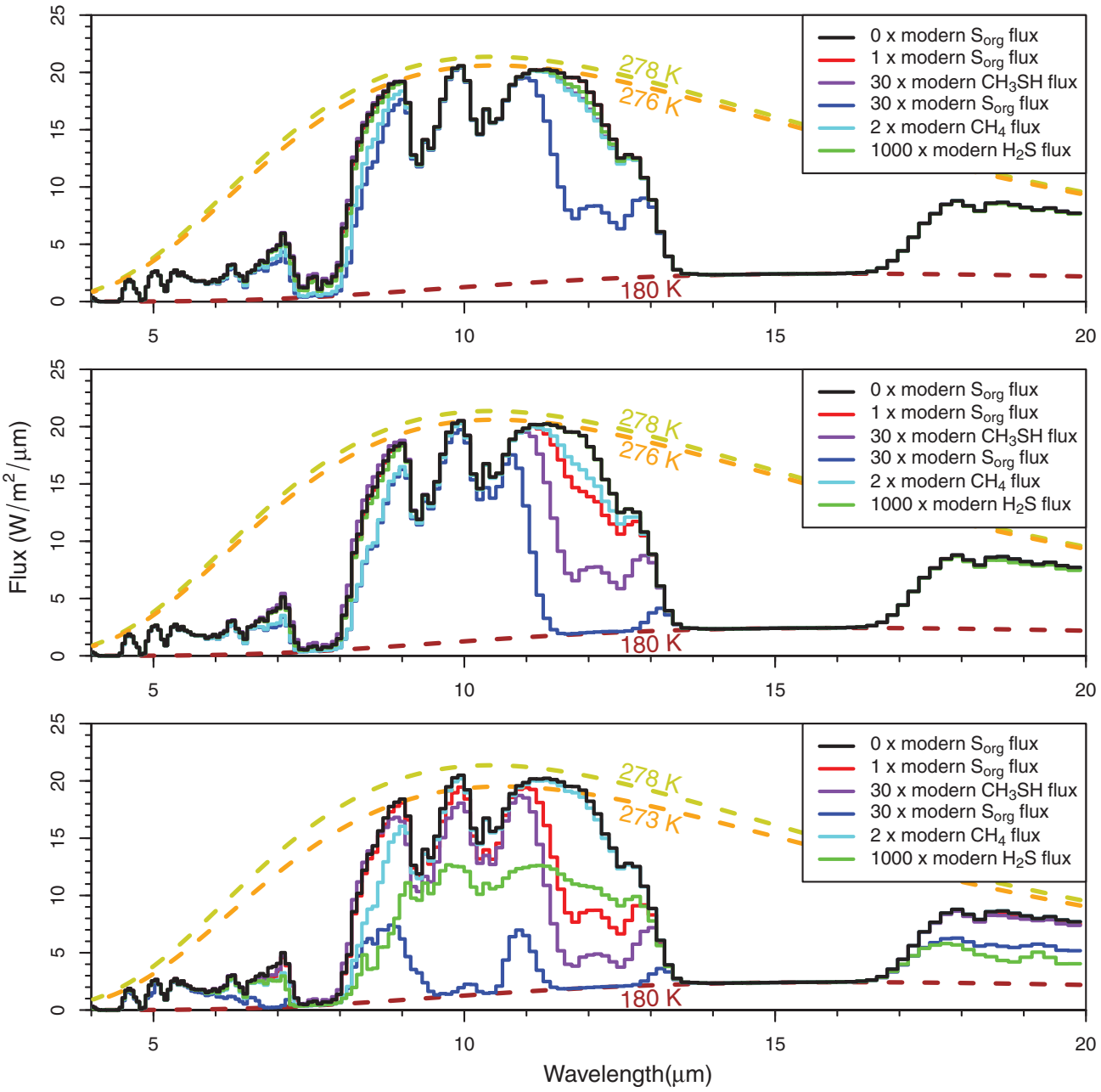

FIG. 5. Spectra for planets around the Sun (top panel), AD Leo (middle panel), and T3100, a model M dwarf with no chromosphere (bottom panel), all at a spectral resolution of $\lambda/\Delta\lambda \sim 50$. The black curve is a spectrum for a planet with 0 S_{org} flux. The red and blue lines show model spectra for planets with 1 and 30 times the modern S_{org} fluxes. The purple lines show spectra for planets with 30 times the modern day flux of CH_3SH and 0.65 times the modern day flux of CH_4. The cyan lines show spectra with 2 times the modern day flux of CH_4 and 0 S_{org} flux. The green lines show spectra with 1000 times the modern day flux of H_2S and 0 S_{org} flux. The goldenrod, orange, and brown dashed lines represent the Planck function for an object at 278 K (the surface temperature), 276 or 273 K (the highest "color temperature" for the "1 modern S_{org} flux" spectrum), and 180 K (the stratospheric temperature).

feature at 11 μm. Thus, they have a significant impact across a wide wavelength range. However, these features only appeared in model simulations with extremely low UV fluxes (the T3100 case) or in simulations with at least 30-fold increases in the flux rate of all S_{org} gases. On planets around more active stars, these features would only be detectable if the biosphere is much more productive than Earth's biosphere or if the organisms living on the planet have high concentrations of sulfur in their proteins. Even planets with an active mercaptogen community would not produce these features unless that community produces CH_3SH at a rate that is greater than 30 times the modern-day CH_3SH flux from the oceans.

Additional confusion in interpreting potential arises from the influence of surface temperature. Discriminating between planets with absorption by S_{org} species and planets with lower surface temperatures may prove problematic, as the S_{org} gases all absorb in the 8–12 μm "atmospheric window" wavelength region. This is a part of the spectrum that some

have suggested could be used to discern surface temperatures, because on modern-day Earth that region is the most transparent to the IR radiation emitted by the surface of Earth. However, an increase in greenhouse gases that absorb photons in this region (including S_{org} species) will increase its opacity, thereby decreasing the effectiveness with which the surface temperature can be ascertained.

The quantitative effect of S_{org} absorption on inferred planetary temperature is shown by the dashed curves in Fig. 5. Here the model spectra, which are cloud free, have been degraded to the spectral resolution goal for TPF-I and are shown with blackbody spectra at three temperatures: (1) 180 K, the stratospheric temperature in our model (drawn in brown); (2) 278 K, the surface temperature in our model (drawn in goldenrod); and (3) either 276 K (top, middle) or 273 K (bottom), the maximum temperature derived for 1 MDF S_{org} case within the window region of the model spectrum (drawn in orange). Figure 5 shows that the S_{org} gas absorption, in addition to weak water vapor absorption, increases the opacity of the atmosphere in the atmospheric window sufficiently that the majority of the radiation sensed comes from higher, colder regions of the planet's troposphere. The discrepancy between actual surface temperature (278 K) and maximum observed temperature is as much as 8 K for the highest S_{org} fluxes and lowest UV fluxes. This will increase the planet's greenhouse effect but decrease the effectiveness with which the surface temperature can be sensed remotely. This effect is from atmospheric absorption alone and does not account for the atmospheric column-truncating effects of clouds or hazes, which for an unresolved Earth-like planet can further reduce the measured brightness temperature in the window region.

Obtaining the best possible estimates of planetary surface temperatures for extrasolar planets of unknown composition will therefore require sufficient spectral wavelength range and resolution to identify non-Earth-like atmospheric window regions, and good estimates of planetary composition and the presence of cloud or aerosol cover. These measurements, combined with atmospheric modeling, will be crucial for understanding limitations on planetary temperature retrieval from MIR spectra for planets with atmospheric characteristics unlike those of modern Earth. For anoxic atmospheres, it is important to be able to detect S_{org} absorption features at wavelengths shortward of the window region. Absorption by DMS and DMDS between 6 and 9 μm provides an extra constraint on the abundance of these gases. Similarly, the C_2H_6 feature could be used in conjunction with photochemical models to further constrain the S_{org} flux rates. The atmospheric S_{org} inventory could then be input to a climate model to calculate self-consistent surface temperatures and spectra. A fairly comprehensive characterization of an anoxic atmosphere could therefore be achieved with spectra from 6 to 13 μm (and preferably down to 5 μm and out to 20 μm to help constrain water abundances) at a spectral resolution of at least 20 and a S/N greater than 15. These baseline parameters are consistent with the current requirement goals for the TPF-I mission concept.

5. Conclusions

In this paper, we have shown that an anoxic biosphere could be detected over interstellar distances by searching for organic S species produced by biology. On planets orbiting Sun-type stars, S_{org} fluxes at 30 times modern-day levels could be detected in the form of elevated C_2H_6/CH_4 ratios that are a photochemical by-product of S_{org} gases. On planets around M dwarfs such as AD Leo, detection of heightened C_2H_6/CH_4 ratios is possible at present-day S_{org} fluxes. Features caused directly by S_{org} gases may be observable on planets that have much higher S_{org} fluxes or on planets orbiting M dwarfs that exhibit low amounts of stellar activity, or both. An important caveat to this work is that aerosols, including water clouds, hydrocarbon aerosols, sulfate aerosols, and S_8 particles, were not considered in the spectral portion of this study but may impact the ability to detect these species.

The detection of any of these features will require an instrument with spectral resolution $R > 20$, broad coverage of the IR spectrum (6–14 μm), and low total noise levels (S/N > 15 or noise $< 1\,W/m^2/\mu m$). Current expected performance levels for TPF-I meet these requirements (Lawson *et al.*, 2007). The use of models to interpret the spectra will also be required in order to separate the effects of surface temperature, organic sulfur gases, and other atmospheric constituents on the planetary spectrum.

Despite the difficulties involved, the benefits offered by such a search are considerable. By including organic sulfur species in our repertoire of remotely detectable biosignatures, the detection of life on some planets may also come with rudimentary lessons on the composition of that planet's biosphere. Thus, this work supports exoplanet characterization missions with a wavelength range and spectral resolution sufficient to detect C_2H_6 and the organic sulfur gases discussed above.

Acknowledgments

The quality of this manuscript was improved by the useful critiques of three reviewers. This work was performed as part of the NASA Astrobiology Institute's Virtual Planetary Laboratory, supported by the National Aeronautics and Space Administration through the NASA Astrobiology Institute under solicitation No. NNH05ZDA001C. Additional support was provided by the Pennsylvania State Astrobiology Research Center, supported by the National Aeronautics and Space Administration through the NASA Astrobiology Institute under grant number NNA09DA76A. S.D.D.-G. acknowledges additional support from the Astrobiology NSF IGERT grant at the University of Washington. M.C. and S.D.D.-G. acknowledge additional support from the NASA Postdoctoral Program. J.F.K. acknowledges additional support from NASA's Exobiology and Evolutionary Biology Program.

Abbreviations

DMS, dimethyl sulfide; DMDS, dimethyl disulfide; MDF, modern-day flux; S/N, signal-to-noise ratio; TPF-I, Terrestrial Planet Finder Interferometer.

References

Adachi, H., Basco, N., and James, D.G.L. (1981) The acetyl radicals CH_3CO^- and CD_3CO^- studied by flash photolysis and kinetic spectroscopy. *International Journal of Chemical Kinetics* 13:1251–1276.

Albers, E.A., Hoyermann, K., Wagner, H.G., and Wolfrum, J. (1969) Study of the reaction of ammonia with oxygen atoms. *Symposium (International) on Combustion* 12:313–321.

Allard, F., Hauschildt, P.H., Alexander, D.R., and Starrfield, S. (1997) Model atmospheres of very low mass stars and brown dwarfs. *Annu Rev Astron Astrophys* 35:137–177.

Allen, M., Yung, Y.L., and Gladstone, G.R. (1992) The relative abundance of ethane to acetylene in the jovian stratosphere. *Icarus* 100:527–533.

Amano, A., Yamada, M., Hashimoto, K., and Sugiura, K. (1983) Kinetic feature of the reaction between methanethiol and hydrogen atoms. *Nippon Kagaku Kaishi* 12:385–393.

Anastasi, C., Broomfield, M., Nielsen, O.J., and Pagsberg, P. (1991) Ultraviolet absorption spectra and kinetics of CH_3S and CH_2SH radicals. *Chem Phys Lett* 182:643–648.

Arthur, N.L. and Lee, M. (1976) Reactions of methyl radicals. I. Hydrogen abstraction from dimethyl sulphide. *Aust J Chem* 29:1483–1492.

Ashfold, M.N.R., Fullstone, M.A., Hancock, G., and Ketley, G.W. (1981) Singlet methylene kinetics: direct measurements of removal rates of $\tilde{a}^1A_1$ and $\tilde{b}^1B_1$ CH_2 and CD_2. *Chem Phys* 55:245–257.

Atkinson, R., Baulch, D.L., Cox, R.A., Hampson, J.R.F., Kerr, J.A., and Troe, J. (1989) Evaluated kinetic and photochemical data for atmospheric chemistry: supplement III. IUPAC Subcommittee on Gas Kinetic Data Evaluation for Atmospheric Chemistry. *Journal of Physical and Chemical Reference Data* 18:881–1097.

Atkinson, R., Baulch, D.L., Cox, R.A., Crowley, J.N., Hampson, R.F., Hynes, R.G., Jenkin, M.E., Rossi, M.J., and Troe, J. (2004) Evaluated kinetic and photochemical data for atmospheric chemistry: Volume I—gas phase reactions of O_X, HO_X, NO_X and SO_X species. *Atmos Chem Phys* 4:1461–1738.

Basco, N. and Pearson, A.E. (1967) Reactions of sulphur atoms in presence of carbon disulphide, carbonyl sulphide, and nitric oxide. *Transactions of the Faraday Society* 63:2684–2694.

Baughcum, S.L. and Oldenborg, R.C. (1984) *Measurement of the* $C_2(a^3\Pi_u)$ *and* $C_2(X^1\Sigma]_g^+)$ *Disappearance Rates with* O_2 *from 298 to 1300 Kelvin,* Oxford University Press, Cary, NC.

Baulch, D.L., Drysdale, D.D., and Home, D.G. (1976) *Evaluated Kinetic Data for High Temperature Reactions,* Butterworths, London.

Baulch, D.L., Cobos, C.J., Cox, R.A., Esser, C., Frank, P., Just, T., Kerr, J.A., Pilling, M.J., Troe, J., Walker, R.W., and Warnatz, J. (1992) Evaluated kinetic data for combustion modelling. *Journal of Physical and Chemical Reference Data* 21:411–734.

Baulch, D.L., Cobos, C.J., Cox, R.A., Frank, P., Hayman, G., Just, T., Kerr, J.A., Murrells, T., Pilling, M.J., Troe, J., Walker, R.W., and Warnatz, J. (1994) Evaluated kinetic data for combustion modeling. Supplement I. *Journal of Physical and Chemical Reference Data* 23:847–848.

Becker, K.H., Engelhardt, B., Wiesen, P., and Bayes, K.D. (1989) Rate constants for $CH(X^2\Pi)$ reactions at low total pressures. *Chem Phys Lett* 154:342–348.

Benson, S.W. and Haugen, G.R. (1967) Mechanism of the high-temperature reactions between acetylene and hydrogen. *The Journal of Physical Chemistry* 71:4404–4411.

Berman, M.R., Fleming, J.W., Harvey, A.B., and Lin, M.C. (1982) Temperature dependence of CH radical reactions with O_2, NO, CO and CO_2. *Symposium (International) on Combustion* 19:73–79.

Berndt, M.E., Allen, D.E., and Seyfried, W.E. (1996) Reduction of CO_2 during serpentinization of olivine at 300 degrees C and 500 bar. *Geology* 24:351–354.

Böhland, T., Dõbe, S., Temps, F., and Wagner, H.G. (1985) Kinetics of the reactions between $CH_2(\tilde{\chi}^3B_1)$-radicals and saturated hydrocarbons in the temperature range $296\,K \le T \le 707\,K$. *Berichte der Bunsengesellschaft für physikalische Chemie* 89:1110–1116.

Braun, W., Bass, A.M., and Pilling, M. (1970) Flash photolysis of ketene and diazomethane: the production and reaction kinetics of triplet and singlet methylene. *J Chem Phys* 52:5131–5143.

Brown, R.L. and Laufer, A.H. (1981) Calculation of activation energies for hydrogen-atom abstractions by radicals containing carbon triple bonds. *The Journal of Physical Chemistry* 85:3826–3828.

Butler, J.E., Fleming, J.W., Goss, L.P., and Lin, M.C. (1981) Kinetics of CH radical reactions with selected molecules at room temperature. *Chem Phys* 56:355–365.

Campbell, I.M. and Gray, C.N. (1973) Rate constants for $O(^3P)$ recombination and association with $N(^4S)$. *Chem Phys Lett* 18:607–609.

Canfield, D.E. (2005) The early history of atmospheric oxygen: homage to Robert A. Garrels. *Annu Rev Earth Planet Sci* 33: 1–36.

Choi, Y.M. and Lin, M.C. (2005) Kinetics and mechanisms for reactions of HNO with CH_3 and C_6H_5 studied by quantum-chemical and statistical-theory calculations. *International Journal of Chemical Kinetics* 37:261–274.

Chung, K., Calvert, J.G., and Bottenheim, J.W. (1975) The photochemistry of sulfur dioxide excited within its first allowed band (3130 Å) and the "forbidden" band (3700–4000 Å). *International Journal of Chemical Kinetics* 7:161–182.

Crisp, D. (1997) Absorption of sunlight by water vapor in cloudy conditions: a partial explanation for the cloud absorption anomaly. *Geophys Res Lett* 24:571–574.

DeMore, W.B. and Yung, Y.L. (1982) Catalytic processes in the atmospheres of Earth and Venus. *Science* 217:1209–1213.

Des Marais, D.J., Harwit, M.O., Jucks, K.W., Kasting, J.F., Lin, D.N.C., Lunine, J.I., Schneider, J., Seager, S., Traub, W.A., and Woolf, N.J. (2002) Remote sensing of planetary properties and biosignatures on extrasolar terrestrial planets. *Astrobiology* 2:153–181.

DeWitt, H.L., Hasenkopf, C.A., Trainer, M.G., Farmer, D.K., Jimenez, J.L., McKay, C.P., Toon, O.B., and Tolbert, M.A. (2010) The formation of sulfate and elemental sulfur aerosols under varying laboratory conditions: implications for early Earth. *Astrobiology* 10:773–781.

Domagal-Goldman, S.D., Kasting, J.F., Johnston, D.T., and Farquhar, J. (2008) Organic haze, glaciations and multiple sulfur isotopes in the Mid-Archean era. *Earth Planet Sci Lett* 269:29–40.

Donovan, R.J. and Husain, D. (1970) Recent advances in the chemistry of electronically excited atoms. *Chem Rev* 70:489–516.

Du, S., Francisco, J.S., Shepler, B.C., and Peterson, K.A. (2008) Determination of the rate constant for sulfur recombination by quasiclassical trajectory calculations. *J Chem Phys* 128, doi:10.1063/1.2919569.

Ekwenchi, M.M., Jodhan, A., and Strausz, O.P. (1980) Reaction of hydrogen atoms with dimethyldisulfide. *International Journal of Chemical Kinetics* 12:431–438.

European Space Agency. (2010) *ESA—Space Science—Darwin,* European Space Agency, Paris. Available online at http://www.esa.int/science/darwin.

Fahr, A., Laufer, A., Klein, R., and Braun, W. (1991) Reaction rate of determinations of vinyl radical reactions with vinyl, methyl, and hydrogen atoms. *The Journal of Physical Chemistry* 95:3218–3224.

Farquhar, J. and Wing, B.A. (2003) Multiple sulfur isotopes and the evolution of the atmosphere. *Earth Planet Sci Lett* 213:1–13.

Farquhar, J., Peters, M., Johnston, D.T., Strauss, H., Masterson, A., Wiechert, U., and Kaufman, A.J. (2007) Isotopic evidence for Mesoarchaean anoxia and changing atmospheric sulphur chemistry. *Nature* 449:706–709.

Fenimore, C.P. (1969) Destruction of methane in water gas by reaction of CH_3 and OH radicals. *Symposium (International) on Combustion* 12:463–467.

Gehring, Mv., Hoyermann, K., Wagner, H.G., and Wolfrum. J. (1971) Die reaktion von atomarem wasserstoff mit hydrazin. *Berichte der Bunsengesellschaft für physikalische Chemie* 75:1287–1294.

Giguere, P.T. and Huebner, W.F. (1978) A model of comet comae. I—Gas-phase chemistry in one dimension. *Astrophys J* 223:638–654.

Gladstone, G.R., Allen, M., and Yung, Y.L. (1996) Hydrocarbon photochemistry in the upper atmosphere of Jupiter. *Icarus* 119:1–52.

Gordon, S., Mulac, W., and Nangia, P. (1971) Pulse radiolysis of ammonia gas. II. Rate of disappearance of the $NH_2(X^2B_1)$ radical. *The Journal of Physical Chemistry* 75:2087–2093.

Hampson, R.F. and Garvin, D. (1977) Evaluation and compilation of reaction rate data. *The Journal of Physical Chemistry* 81:2317–2319.

Haqq-Misra, J.D., Domagal-Goldman, S.D., Kasting, P.J., and Kasting, J.F. (2008) A revised, hazy methane greenhouse for the Archean Earth. *Astrobiology* 8:1127–1137.

Hills, A.J., Cicerone, R.J., Calvert, J.G., and Birks, J.W. (1987) Kinetics of the reactions of diatomic sulfur with atomic oxygen, molecular oxygen, ozone, nitrous oxide, nitric oxide, and nitrogen dioxide. *The Journal of Physical Chemistry* 91:1199–1204.

Holland, H.D. (1984) *The Chemical Evolution of the Atmosphere and Oceans,* Princeton University Press, Princeton, NJ.

Homann, K.H. and Wellmann, C. (1983) Kinetics and mechanism of hydrocarbon formation in the system $C_2H_2/O/H$ at temperatures up to 1300 K. *Berichte der Bunsengesellschaft für physikalische Chemie* 87:609–616.

Hoyermann, K., Loftfield, N.S., Sievert, R., and Wagner, H.G. (1981) Mechanisms and rates of the reactions of CH_3O and CH_2OH radicals with H atoms. *Symposium (International) on Combustion* 18:831–842.

Huebner, W.F. and Giguere, P.T. (1980) A model of comet comae. II—Effects of solar photodissociative ionization. *Astrophys J* 238:753–762.

Intergovernmental Panel on Climate Change. (2007) *Climate Change 2007: Synthesis Report. Contribution of Working Groups I, II and III to the Fourth Assessment Report of the Intergovernmental Panel on Climate Change*, edited by R.K. Pachauri, A. Reisinger, and the Core Writing Team, Intergovernmental Panel on Climate Change, Geneva.

Jasper, A.W., Klippenstein, S.J., Harding, L.B., and Ruscic, B. (2007) Kinetics of the reaction of methyl radical with hydroxyl radical and methanol decomposition. *J Phys Chem A* 111:3932–3950.

Jet Propulsion Laboratory. (2010) *Planet Quest: Missions—Terrestrial Planet Finder,* Jet Propulsion Laboratory, Pasadena, CA. Available online at http://planetquest.jpl.nasa.gov/TPF.

Kaltenegger, L. and Sasselov, D. (2010) Detecting planetary geochemical cycles on exoplanets: atmospheric signatures and the case of SO_2. *Astrophys J* 708:1162–1167.

Kaltenegger, L., Traub, W.A., and Jucks, K.W. (2007) Spectral evolution of an Earth-like planet. *Astrophys J* 658:598–616.

Kaltenegger, L., Henning, W.G., and Sasselov, D. (2010) Detecting volcanism on extrasolar planets. *Astron J* 140:1370–1380.

Kasting, J.F. (1982) Stability of ammonia in the primitive terrestrial atmosphere. *J Geophys Res* 87:3091–3098.

Kasting, J.F. (1990) Bolide impacts and the oxidation state of carbon in the Earth's early atmosphere. *Orig Life Evol Biosph* 20:199–231.

Kasting, J.F. (2005) Methane and climate during the Precambrian era. *Precambrian Res* 137:119–129.

Kasting, J.F. and Ackerman, T.P. (1985) High atmospheric NO_X levels and multiple photochemical steady-states. *J Atmos Chem* 3:321–340.

Kasting, J.F. and Catling, D. (2003) Evolution of a habitable planet. *Annu Rev Astron Astrophys* 41:429–463.

Kasting, J.F., Liu, S.C., and Donahue, T.M. (1979) Oxygen levels in the prebiological atmosphere. *J Geophys Res* 84:3097–3107.

Kasting, J.F., Zahnle, K.J., and Walker, J.C.G. (1983) Photochemistry of methane in the Earth's early atmosphere. *Precambrian Res* 20:121–148.

Kasting, J.F., Pavlov, A.A., and Siefert, J.L. (2001) A coupled ecosystem-climate model for predicting the methane concentration in the archean atmosphere. *Orig Life Evol Biosph* 31: 271–285.

Kerr, J.A. and Trotman-Dickenson, A.F. (1957) The reactions of methyl radicals with thiols. *The Journal of the Chemical Society* 79:3322.

Kettle, A.J., Rhee, T.S., von Hobe, M., Poulton, A., Aiken, J., and Andreae, M.O. (2001) Assessing the flux of different volatile sulfur gases from the ocean to the atmosphere. *J Geophys Res* 106:12193–12209.

Kharecha, P., Kasting, J.F., and Siefert, J.L. (2005) A coupled atmosphere-ecosystem model of the early Archean Earth. *Geobiology* 3:53–76.

Krasnoperov, L.N., Chesnokov, E.N., Stark, H., and Ravishankara, A.R. (2004) Unimolecular dissociation of formyl radical, $HCO \rightarrow H + CO$, studied over 1–100 bar pressure range. *J Phys Chem A* 108:11526–11536.

Kuhn, W.R. and Atreya, S.K. (1979) Ammonia photolysis and the greenhouse effect in the primordial atmosphere of the earth. *Icarus* 37:207–213.

Kurbanov, M.A. and Mamedov, K.H.F. (1995) *The Role of the Reaction of $CO + SH \rightarrow COS + H$ in Hydrogen Formation in the Course of Interaction between CO and H_2S,* Maik Nauka/Interperiodica, Moscow.

Lam, W.W., Yokota, T., Safarik, I., and Strausz, O.P. (1989) Photolysis of and reactions of hydrogen atoms with ethanethiol. *J Photochem Photobiol A Chem* 47:47–63.

Lander, D.R., Unfried, K.G., Glass, G.P., and Curl, R.F. (1990) *Rate Constant Measurements of C_2H with CH_4, C_2H_6, C_2H_4, D_2, and CO,* American Chemical Society, Washington DC.

Laufer, A. (1981) Kinetics of gas phase reactions of methylene. *Research on Chemical Intermediates* 4:225–257.

Laufer, A.H., Gardner, E.P., Kwok, T.L., and Yung, Y.L. (1983) Computations and estimates of rate coefficients for hydrocarbon reactions of interest to the atmospheres of outer Solar System. *Icarus* 56:560–567.

Lawson, P.R., Lay, O.P., Johnston, K.J., and Beichman, C.A. (2007) *Terrestrial Planet Finder Interferometer Science Working Group Report,* Jet Propulsion Laboratory, California Institute of Technology, Pasadena, CA.

Lederberg, J. (1965) Signs of life: criterion-system of exobiology. *Nature* 207:9–13.

Lee, J.H., Stief, L.J., and Timmons, R.B. (1977) Absolute rate parameters for the reaction of atomic hydrogen with carbonyl sulfide and ethylene episulfide. *J Chem Phys* 67:1705–1709.

Lee, L.C. (1980) CN($A^2\Pi_i \rightarrow X^2\Sigma^+$) and CN($B^2\Sigma^+ \rightarrow X^2\Sigma^+$) yields from HCN photodissociation. *J Chem Phys* 72:6414–6421.

Lightfoot, P.D. and Pilling, M.J. (1987) Temperature and pressure dependence of the rate constant for the addition of hydrogen atoms to ethylene. *The Journal of Physical Chemistry* 91:3373–3379.

Liu, Y., Wang, W.L., Wang, W.N., Luo, Q., and Li, Q.S. (2006) Density functional theory study on the biradical reaction between CH_3S and HCS. *Acta Chimica Sinica* 17:1785–1792.

Lloyd, A.C. (1974) Evaluated and estimated kinetic data for phase reactions of the hydroperoxyl radical. *International Journal of Chemical Kinetics* 6:169–228.

Lovelock, J.E. (1965) A physical basis for life detection experiments. *Nature* 207:568–570.

Martinez, R.I. and Herron, J.T. (1983) Methyl thiirane: kinetic gas-phase titration of sulfur atoms in S_XO_Y systems. *International Journal of Chemical Kinetics* 15:1127–1132.

Matsumi, Y., Tonokura, K., Inagaki, Y., and Kawasaki, M. (1993) Isotopic branching ratios and translational energy release of hydrogen and deuterium atoms in reaction of oxygen (^{1}D) atoms with alkanes and alkyl chlorides. *The Journal of Physical Chemistry* 97:6816–6821.

McEwan, M.J. and Phillips, L.F. (1975) *Chemistry of the Atmosphere,* Wiley/Halsted Press, New York.

Meadows, V.S. and Crisp, D. (1996) Ground-based near-infrared observations of the Venus nightside: the thermal structure and water abundance near the surface. *J Geophys Res* 101:4595–4622.

Messing, I., Filseth, S.V., Sadowski, C.M., and Carrington, T. (1981) Absolute rate constants for the reactions of CH with O and N atoms. *J Chem Phys* 74:3874–3881.

Michael, J.V., Nava, D.F., Payne, W.A., and Stief, L.J. (1979) Absolute rate constants for the reaction of atomic hydrogen with ketene from 298 to 500 K. *J Chem Phys* 70:5222–5227.

Miller, J.A., Mitchell, R.E., Smooke, M.D., and Kee, R.J. (1982) Toward a comprehensive chemical kinetic mechanism for the oxidation of acetylene: comparison of model predictions with results from flame and shock tube experiments. *Symposium (International) on Combustion* 19:181–196.

Moran, J.J., House, C.H., Vrentas, J.M., and Freeman, K. (2008) Methyl sulfide production by a novel carbon monoxide metabolism in *Methanosarcina acetivorans*. *Appl Environ Microbiol* 74:540–542.

Niki, H., Maker, P.D., Savage, C.M., and Breitenbach, L.P. (1978) Relative rate constants for the reaction of hydroxyl radical with aldehydes. *The Journal of Physical Chemistry* 82:132–134.

Okabe, H. (1983) Photochemistry of acetylene at 1849 Å. *J Chem Phys* 78:1312–1317.

Pavlov, A.A., Brown, L.L., and Kasting, J.F. (2001) UV shielding of NH_3 and O_2 by organic hazes in the Archean atmosphere. *J Geophys Res* 106:23267–23287.

Peng, J., Hu, X., and Marshall, P. (1999) Experimental and *ab initio* investigations of the kinetics of the reaction of H atoms with H_2S. *J Phys Chem A* 103:5307–5311.

Perry, R.A. and Williamson, D. (1982) Pressure and temperature dependence of the OH radical reaction with acetylene. *Chem Phys Lett* 93:331–334.

Pilcher, C.B. (2003) Biosignatures of early earths. *Astrobiology* 3:471–486.

Pitts, W.M., Pasternack, L., and McDonald, J.R. (1982) Temperature dependence of the $C_2(X^1\Sigma_g^+)$ reaction with H_2 and CH_4 and $C_2(X^1\Sigma_g^+)$ and $a^3\Pi_u$ equilibrated states) with O_2. *Chem Phys* 68:417–422.

Prasad, S.S. and Huntress, W.T., Jr. (1980) A model for gas phase chemistry in interstellar clouds. I—The basic model, library of chemical reactions, and chemistry among C, N, and O compounds. *Astrophys J Suppl Ser* 43:1–35.

Raymond, S.N., Mandell, A.M., and Sigurdsson, S. (2006) Exotic Earths: forming habitable worlds with giant planet migration. *Science* 313:1413–1416.

Robie, D.C., Arepalli, S., Presser, N., Kitsopoulos, T., and Gordon, R.J. (1990) The intramolecular kinetic isotope effect for the reaction O(^{3}P) + HD. *J Chem Phys* 92:7382–7393.

Robinson, T.D., Meadows, V.S., Crisp, D., Deming, D., A'Hearn, M.F., Charbonneau, D., Livengood, T.A., Seager, S., Barry, R.K., Hearty, T., Hewagama, T., Lisse, C.M., McFadden, L.A., and Wellnitz, D.D. (2011) Earth as an extrasolar planet: Earth model validation using EPOXI Earth observations. *Astrobiology* 11.

Romani, P.N., Bishop, J., Bezard, B., and Atreya, S. (1993) Methane photochemistry on Neptune—ethane and acetylene mixing ratios and haze production. *Icarus* 106:442–463.

Rothman, L.S., Jacquemart, D., Barbe, A., Chris Benner, D., Birk, M., Brown, L.R., Carleer, M.R., Chackerian, J.C., Chance, K., Coudert, L.H., Dana, V., Devi, V.M., Flaud, J.-M., Gamache, R.R., Goldman, A., Hartmann, J.-M., Jucks, K.W., Maki, A.G., Mandin, J.-Y., Massie, S.T., Orphal, J., Perrin, A., Rinsland, C.P., Smith, M.A.H., Tennyson, J., Tolchenov, R.N., Toth, R.A., Vander Auwera, J., Varanasi, P., and Wagner, G. (2005) The HITRAN 2004 molecular spectroscopic database. *J Quant Spectrosc Radiat Transf* 96:139–204.

Sagan, C., Thompson, W.R., Carlson, R., Gurnett, D., and Hord, C. (1993) A search for life on Earth from the Galileo spacecraft. *Nature* 365:715–721.

Sander, S.P., Friedl, R.R., Golden, D.M., Kurylo, M.J., Moortgat, G.K., Keller-Rudek, H., Wine, P.H., Ravishankara, A.R., Kolb, C.E., Molina, M.J., Finlayson-Pitts, B.J., Huie, R.E., and Orkin, V.L. (2006) Chemical kinetics and photochemical data for use in atmospheric studies : evaluation number 15, JPL Publication 06-2, Jet Propulsion Laboratory, California Institute of Technology, Pasadena, CA.

Schofield, K. (1973) Evaluated chemical kinetic rate constants for various gas phase reactions. *Journal of Physical and Chemical Reference Data* 2:25–84.

Schopf, J.W., editor. (1983) *Earth's Earliest Biosphere: Its Origin and Evolution,* Princeton University Press, Princeton.

Segura, A., Kasting, J.F., Meadows, V., Cohen, M., Scalo, J., Crisp, D., Butler, R.A.H., and Tinetti, G. (2005) Biosignatures from Earth-like planets around M dwarfs. *Astrobiology* 5:706–725.

Sharpe, S.W., Johnson, T.J., Sams, R.L., Chu, P.M., Rhoderick, G.C., and Johnson, P.A. (2004) Gas-phase databases for quantitative infrared spectroscopy. *Appl Spectrosc* 58:1452–1461.

Shum, L.G.S. and Benson, S.W. (1985) The pyrolysis of dimethyl sulfide, kinetics and mechanism. *International Journal of Chemical Kinetics* 17:749–761.

Singleton, D.L. and Cvetanovic, R.J. (1988) Evaluated chemical kinetic data for the reactions of atomic oxygen O(^{3}P) with sulfur containing compounds. *Journal of Physical and Chemical Reference Data* 17:1377–1437.

Stachnik, R.A. and Molina, M.J. (1987) Kinetics of the reactions of mercapto radicals with nitrogen dioxide and oxygen. *The Journal of Physical Chemistry* 91:4603–4606.

Stephens, J.W., Hall, J.L., Solka, H., Yan, W.B., Curl, R.F., and Glass, G.P. (1987) Rate constant measurements of reactions of

ethynyl radical with hydrogen, oxygen, acetylene and nitric oxide using color center laser kinetic spectroscopy. *The Journal of Physical Chemistry* 91:5740–5743.

Stief, L.J. and Payne, W.A. (1976) Absolute rate parameters for the reaction of atomic hydrogen with hydrazine. *J Chem Phys* 64:4892–4896.

Sun, F., DeSain, J.D., Scott, G., Hung, P.Y., Thompson, R.I., Glass, G.P., and Curl, R.F. (2001) Reactions of NH_2 with NO_2 and of OH with NH_2O. *J Phys Chem A* 105:6121–6128.

New Worlds Observer Team. (2010) *New Worlds*. New Worlds Observer Team, Boulder, CO. Available online at http://newworlds.colorado.edu.

Toon, O.B., Kasting, J.F., Turco, R.P., and Liu, M.S. (1987) The sulfur cycle in the marine atmosphere. *J Geophys Res* 92:943–963.

Trainer, M.G., Pavlov, A.A., DeWitt, H.L., Jimenez, J.L., McKay, C.P., Toon, O.B., and Tolbert, M.A. (2006) Organic haze on Titan and the early Earth. *Proc Natl Acad Sci USA* 103:18035–18042.

Tsang, W. and Hampson, R.F. (1986) Chemical kinetic data base for combustion chemistry. Part I. Methane and related compounds. *Journal of Physical and Chemical Reference Data* 15:1087–1279.

Tsang, W. and Herron, J.T. (1991) Chemical kinetic data base for propellant combustion I. Reactions involving NO, NO_2, HNO, HNO_2, HCN and N_2O. *Journal of Physical and Chemical Reference Data* 20:609–663.

Turco, R.P., Whitten, R.C., and Toon, O.B. (1982) Stratospheric aerosols: observation and theory. *Reviews of Geophysics and Space Physics* 20:233–280.

Turnipseed, A.A., Barone, S.B., and Ravishankara, A.R. (1996) Reaction of OH with dimethyl sulfide. 2. Products and mechanisms. *The Journal of Physical Chemistry* 100:14703–14713.

Vance, S., Christensen, L.E., Webster, C.R., and Sung, K. (2011) Volatile organic sulfur compounds as biomarkers complementary to methane: infrared absorption spectroscopy of CH_3SH enables in-situ measurements on Earth and Mars. *Planet Space Sci* 59:299–303.

Vaghjiani, G.L. and Ravishankara, A.R. (1990) Photodissociation of H_2O_2 and CH_3OOH at 248 nm and 298 K—quantum yields for OH, $O(^3P)$ and $H(^2S)$. *J Chem Phys* 92:996–1003.

Wagner, A.F. and Wardlaw, D.M. (1988) Study of the recombination reaction methyl + methyl → ethane. 2. Theory. *The Journal of Physical Chemistry* 92:2462–2471.

Walker, J.C.G. (1977) *Evolution of the Atmosphere,* Macmillan, New York.

Warnatz, J. (1984) Rate coefficients in the C/H/O system. In *Combustion Chemistry,* edited by W.C. Gadner Jr., Springer-Verlag, New York, pp 197–360.

Washida, N. (1981) Reaction of ethanol and $CH_3CH(OH)$ radicals with atomic and molecular oxygen. *J Chem Phys* 75:2715–2722.

Watkins, K.W. and Word, W.W. (1974) Addition of methyl radicals to carbon monoxide: chemically and thermally activated decomposition of acetyl radicals. *International Journal of Chemical Kinetics* 6:855–873.

Wen, J.-S., Pinto, J.P., and Yung, Y.L. (1989) Photochemistry of CO and H_2O—analysis of laboratory experiments and applications to the prebiotic Earth's atmosphere. *J Geophys Res* 94:14957–14970.

Westall, F. (2005) Evolution: life on the early Earth: a sedimentary view. *Science* 308:366–367.

Whytock, D.A., Payne, W.A., and Stief, L.J. (1976) Rate of the reaction of atomic hydrogen with propyne over an extended pressure and temperature range. *J Chem Phys* 65:191–195.

Wine, P.H., Chameides, W.L., and Ravishankara, A.R. (1981) Potential role of CS_2 photooxidation in tropospheric sulfur chemistry. *Geophys Res Lett* 8:543–546.

Woiki, D. and Roth, P. (1995) Oxidation of S and SO by O_2 in high-temperature pyrolysis and photolysis reaction systems. *International Journal of Chemical Kinetics* 27:59–71.

Yung, Y.L. and Demore, W.B. (1982) Photochemistry of the stratosphere of Venus—implications for atmospheric evolution. *Icarus* 51:199–247.

Yung, Y.L., Allen, M., and Pinto, J.P. (1984) Photochemistry of the atmosphere of Titan—comparison between model and observations. *Astrophys J Suppl Ser* 55:465–506.

Zabarnick, S., Fleming, J.W., and Lin, M.C. (1986) Kinetic study of the reaction $CH(X^2\Pi) + H_2 \leftrightarrow CH_2(X^3B_1) + H$ in the temperature range 372 to 675 K. *J Chem Phys* 85:4373–4376.

Zabarnick, S., Fleming, J.W., and Lin, M.C. (1989) Kinetics of CH radical reactions with N_2O, SO_2, OCS, CS_2, and SF_6. *International Journal of Chemical Kinetics* 21:765–774.

Zahnle, K.J. (1986) Photochemistry of methane and the formation of hydrocyanic acid (HCN) in the Earth's early atmosphere. *J Geophys Res* 91:2819–2834.

Zahnle, K.J. and Kasting, J.F. (1986) Mass fractionation during transonic escape and implications for loss of water from Mars and Venus. *Icarus* 68:462–480.

Zahnle, K.J., Claire, M.W., and Catling, D.C. (2006) The loss of mass-independent fractionation in sulfur due to a Palaeoproterozoic collapse of atmospheric methane. *Geobiology* 4:271–283.

Zhang, Q., Sun, T., Zhou, X., and Wang, W. (2005) Rate parameters and branching ratios for the multiple-channel reaction of dimethyl sulfide DMS with atomic H. *Chem Phys Lett* 414:316–321.

Address correspondence to:
Shawn D. Domagal-Goldman
NASA Headquarters
300 E St. SW
Washington, DC 20056

E-mail: shawn.goldman@gmail.com

Submitted 15 June 2010
Accepted 19 March 2011